ATOMISTIC MODELLING TO STUDY EFFECT OF RADIATION DAMAGE ON NUCLEAR MATERIALS

A Dissertation

Submitted in partial fulfillment of the

requirements for the award of degree

of

MASTER OF TECHNOLOGY

in

MECHANICAL ENGINEERING

(With specialization in Machine Design Engineering)

By

PRASHANT SHARMA (17539008)

DEPARTMENT OF MECHANICAL AND INDUSTRIAL ENGINEERING

INDIAN INSTITUTE OF TECHNOLOGY ROORKEE,

ROORKEE, UTTARAKHAND, INDIA - 247667

MAY 2019

CANDIDATE'S DECLARATION

I hereby declare that the work which is being presented in this Seminar, entitled, "**Atomistic modelling to study effect of radiation damage on nuclear materials** ", in partial fulfilment of the requirement for the award of the degree of Master of Technology in " Machine Design Engineering", submitted in the Department of Mechanical and Industrial Engineering, Indian Institute of Technology, Roorkee under the supervision of **Dr. Avinash Parashar**, Assistant Professor and **Dr. Sanjay H. Upadhyay** , Associate Professor, Department of Mechanical and Industrial Engineering, Indian Institute of Technology, Roorkee, India.

Place: MIED, IIT Roorkee

(Prashant Sharma)
Enrolment No.
17539008

CERTIFICATE

This is to certify that the above statement made by candidate is correct to the best of my knowledge.

…….....

(Dr. Avinash Parashar)
Assistant Professor
MIED, IIT Roorkee

……..

(Dr. Sanjay H. Upadhyay)
Associate Professor
MIED, IIT Roorkee

Department of Mechanical and Industrial Engineering
Indian Institute of Technology,
Roorkee -247677, India

ACKNOWLEDGEMENT

It is my great pleasure in expressing my heartfelt gratitude to my supervisors **Dr. Avinash Parashar**, Assistant Professor and **Dr. Sanjay H. Upadhyay**, Associate Professor, Department of Mechanical and Industrial Engineering, Indian Institute of Technology, Roorkee, for their valuable guidance, direction and infilling support towards completion of this dissertation. I am highly obliged to them for their keen interest, able guidance and encouragement throughout the writing. Working under their guidance is a privilege, great opportunity and an excellent learning experience that I will flourish in my life time.

I take this opportunity to put on records my respects to **Professor BK Gandhi**, HOD Department of Mechanical and Industrial Engineering Indian Institute of Technology Roorkee, for providing various facilities during course of present investigation.

I would like to especially thank my colleagues Ms. Divya Singh, Mr. Bharat Bhushan Sharma, Mr. Akarsh Verma, Mr. Ankur Chaurasia and Mr Saurabh S Sharma for their valuable cooperation, suggestions, help and guidance in completing all tests and dissertation. I am extremely thankful to other professors and my classmates from Department of Mechanical and Industrial Engineering, IIT Roorkee for their kind support, encouragement and cooperation. I remain eternally indebted to my parents, Late. Mr. Om Prakash Sharma and Mrs. Sushila Devi for their uplifting inspiration, guidance and never-ending enthusiasm.

Finally, I would like to express my deepest gratitude to the Almighty for showering blessings on me.

……..

(Prashant Sharma)

Enrollment no: 17539008

Machine Design Engineering

M.Tech IInd Year

ABSTRACT

Niobium (Nb), Zirconium (Zr) and Zr-Nb alloys are commonly used as the structural material in nuclear reactors. Niobium is a rare, soft, malleable, ductile, grey-white metal transition element. Due to superior creep properties and low neutron cross section, Zr-Nb are used for the manufacturing of pressure tubes and fuel cladding in nuclear reactors. Additionally, is used in alloys for nuclear reactors, jets, missiles, cutting tools, pipelines, welding rods and super magnets. On addition of Nb in Zr makes significant improvement in certain properties of Zr like corrosion and creep resistance. In this project molecular dynamics-based simulations were used to study the effect of the irradiation induced microstructural changes in these nuclear materials. Due to time and spatial scale involved in irradiation induced damage, experiments are not feasible, hence atomistic simulations are emerging as viable alternative. In this report, simulations were performed to study the effect of tilt grain boundaries on the point defect formation energies in a bi-crystal of Nb. In order to study the effect of grain boundary configuration on defect formation energies, tilt grain boundaries were generated in the simulation box containing either symmetrical or asymmetrical boundaries between the two crystals of Nb. All the tilt grain boundaries were generated along the [0001] as the tilt axis with different mis-orientation angles. Grain boundary energies were estimated for each mis-orientation angle and a relation is derived between the distance from the grain boundary and defect formation energy. The defect migration energy was also calculated for both symmetrical and asymmetrical tilt grain boundaries. It has been concluded from this part of research project that defect formation energies reduce significantly in vicinity of grain boundaries, which makes these configuration as sink for the radiation induced defects. The results obtained were validated with the help of data available in literature.

TABLE OF CONTENTS

Candidate's Declaration ……..... ii
Acknowledgement ……... iii
Abstract ……..... iv
List of figures ……..…..vii
List of tables ……..……x
Abbreviations……....xi

1. INTRODUCTION……..... **1-18**

1.1 Concept of Radiation Damage …..... 2

1.2 Displacement Cascade…… 3

1.3 Characterizing Techniques ……..... 5

1.4 Modelling techniques for Nb..…… 6

1.4.1 Molecular Dynamics…… 7

1.4.2 Molecular Mechanics……... 8

1.4.3 Monte Carlo…… 9

1.5 Interatomic Potential ……. 9

1.5.1 Pair potential…… 9

1.5.2 Tersoff potential…….. 10

1.5.3 EAM potential……. 10

1.5.4 Empirical potential……. 11

1.5.5 Semi-empirical potential…… 11

1.6 Ensemble……..…….. 12

1.6.1 Type of ensembles…… 12

1.7 Niobium properties and applications……. 13

1.8 Definition of problem…… 17

1.9 Brief description of the work……. 17

2. LITERATURE REVIEW……..... **19-30**

3. SIMULATION DETAILS ……..... **31-34**

3.1. Single crystal of Niobium..... 31

3.2. Niobium bi-crystal simulations……..... 32

3.3. Defect generation and VFE calculation……..…….. 34

4. RESULT AND DISCUSSION…….…….**35-46**

4.1 Variation of VFE with distance from GB……. 40

4.2 Variation of IFE with distance from GB…….. 41

4.3 Variation of min. VFE and GB energy…… 42

4.4 Variation of VFE with mis-orientation angle…..……. 43

4.5 Vacancy Migration Energy……... 44

5. Conclusion and future aspects……**47**

References **48-50**

LIST OF FIGURES

Figure No	Figure Name	Page No
1	Evolution of displacement cascade over time	3
2	Three stages of a displacement cascade (a) Initiation (b) thermal spike (c) relaxation.	4
3	Evolution of displacement cascade and re-arrangement of atoms over layers	5
4	Zirconium crystal bar, Niobium, Zr-Nb alloy tubes	13
5	Rods of steel-niobium alloy.	15
6	Fuel-rod cladding in nuclear powerplants	15
7	Jet engine blades made of Nb based alloy	15
8	High pressure tubes made up of Nb based alloy	16
9	Magnetic Resonance Imaging machine	16
10	Activated slip planes at the onset of plasticity in simulations performed with different PKA energy level.	19
11	Stress-strain response captured with altered PKA energies at a temperature of 10K.	20
12	Stress-strain response captured with altered PKA velocity vectors at a temperature of 10°K.	20
13	Frenkel pairs generated in MD based simulation with respect to (a) simulation box temperature (b) PKA energy	21
14	Frenkel pair generated with respect to PKA velocity vector aligned with various crystal orientation	21
15	Distribution of vacancy (blue atoms) and interstitials (red atoms) in simulation box with respect to simulation box temperatures, PKA energy and PKA velocity vector	22
16	Asymmetrical tilt grain boundary energies at mis-orientation angle of 36.86^{o} as a function of inclination angle (Ø)	23
17	Deviation in GB energy with respect to mis-orientation angle along 〈1 0 0〉 tilt axis.	23

18	Stress-strain curve for 36.86° and 53.13° mis-orientation angle with 〈1 0 0〉 tilt axis at (a) 300 K (b) 1 K	24
19	Dislocation nucleation and growth in STGB for θ = 36.86° mis-orientation angle at 1 K and 300 K (a_1, a_2) Before yield (b_1, b_2) At yield (c_1, c_2) After yield.	24
20	Dislocation nucleation and growth in ATGB for θ = 36.86° and Ø = 26.57° at 1 K and 300 K (a_1, a_2) Before yield (b_1, b_2) At yield (c_1, c_2) After yield.	25
21	Variation in VFE as a function of misorientation angle, and the distance from GB for [0 0 0 1] as tilt axis. (The VFE for an asymmetrical GB (Ø = 10°) is also plotted.)	26
22	The variation in IFE as a function of misorientation angle and distance from GB for [0 0 0 1] as tilt axis. (IFE for an asymmetrical GB (Ø = 10°) is also graphed.)	27
23	The trend of VFE as a function of misorientation angle along tilt axes aligned with [0 0 0 1]. The values specified next to data points correspond to the GB energies at specific misorientation angle.	27
24	The trend of the IFE as a function of misorientation angle along the tilt axes aligned with [0 0 0 1]. The values specified next to data points correspond to GB energies at certain misorientation angle.	28
25	Diagram of generation of symmetric tilt grain boundaries (STGB) and asymmetric tilt grain boundaries (ATGB)	32
26	STGB structures with [0001] as the tilt axis containing mis-orientation angles (a) 25.06^o (b) 43.6^o (c) 53.13^o (d) 67.38 (e) 73.73	35
27	Variation in STGB energy with respect to mis-orientation angle along [0001] tilt axis.	37
28	ATGB structures with misorientation angle (2θ) of 36.86^o along the [0001] tilt axis and inclination angles (Ø) of (a) 30.96^o (b) 36.86^o (c) 43.6^o (d) 53.13^o	38

29	Asymmetrical tilt GB energies at mis-orientation angle of 36.86^{o} as a function of inclination angle (Ø).	39
30	Variation of VFE as a function of mis-orientation angle, and distance from grain boundary for STGB with [0001] as the tilt axis.	40
31	Variation of VFE as a function of the mis-orientation angle, and the distance from the grain boundary for ATGB with [0001] as the tilt axis.	40
32	Variation of VFE as a function of mis-orientation angle, and distance from grain boundary for STGB with [0001] as the tilt axis.	41
33	Variation of VFE as a function of mis-orientation angle, and distance from grain boundary for ASTGB with [0001] as the tilt axis.	42
34	The trend of min. VFE as a function of GB energy for asymmetrical tilt GB with [0001] as the tilt axis.	43
35	Trend of VFE as a function of mis-orientation angle for symmetrical tilt grain boundary tilted along the axis aligned with [0001].	43
36	Trend of VFE as a function of mis-orientation angle for asymmetrical tilt grain boundary tilted along the axis aligned with [0001].	44
37	Minimum vacancy migration path in a bi-crystal of Nb containing a STGB with mis-orientation angle of 36.86 and inclination angle 36.86°.	45
38	Minimum vacancy migration path in a bi-crystal of Nb containing a ATGB with mis-orientation angle of 36.86 and inclination angle 36.86°.	45
39	Minimum vacancy migration path in a bi-crystal of Nb containing a ATGB with mis-orientation angle of 36.86 and inclination angle 36.86°.	46

LIST OF TABLES

Table No	Table Description	Page No
1	Various ensembles used in MD and MC	12
2	Configuration details of symmetric tilt grain boundaries tilted along <0 0 1> axis.	33
3	Configuration details for asymmetric tilt GBs tilted along <0 0 1> for 36.86^{o} mis-orientation angle.	33
4	Variation in GB energy with respect to mis-orientation angle	36
5	ATGB energies with changing inclination angle and a constant mis-orientation angle of 36.86°	39

ABBREVIATIONS

SIA	Self-interstitial atoms
PKA	Primary knock-on atom
FEM	Finite Element Method
MM	Molecular Mechanics
MC	Monte Carlo
EAM	Embedded atom method
Nb	Niobium
Zr	Zirconium
STGB	Symmetrical tilt grain boundary
ATGB	Asymmetrical tilt grain boundary
NEB	Nudged elastic band
VME	Vacancy migration energy
CNA	Common neighbor analysis
VFE	Vacancy formation energy
IFE	Interstitial formation energy
dpa	Displacements per atom
GB	Grain Boundary
LAMMPS	Large Scale Atomic/Molecular Massively Parallel Simulator
OVITO	Open Visualization Tool
CG	Conjugate Gradient

CHAPTER 1

INTRODUCTION

The nuclear power is one of the clean source of energy, emerged in the past few years. The nuclear materials are the structural materials for the nuclear powerplants and they play a vibrant role in fabrication of various components in the nuclear industries. The various nuclear materials possess several unique properties which make them suitable for the number of applications in the various fields. The presence of properties like high ductility, corrosion resistance, hardness and low nuclear cross section makes Zirconium and Niobium based alloys an important constituent element of nuclear industries. Niobium has a variety of applications in the structural component material in nuclear reactors. The use of Niobium in alloys such as Zr-Nb alloy, makes the structure to perform with higher efficiency as compared to the single element structure. The high melting point temperature of the Niobium makes it an important element for the high temperature applications and even to enhance the properties of several other elements by combining with them in the alloy form. Niobium based superalloys are widely used to enhance the operating temperature of the turbine blades. Nb has emerged as a promising candidate to be alloyed with the various materials to enhance their properties. Zr-Nb alloys have a wide use in the fuel rod cladding as well as in pressure tubes of the nuclear reactors. "Gum metal" an alloy of titanium and niobium, exhibit a unique deformation behavior. A significant amount of work has been done by the researchers to study the various defects induced in the nuclear materials and their failure mechanism during their operation. As compared to the single crystal, polycrystalline materials have greater resistance to radiation-induced defects. When the irradiation phenomenon takes place in the nuclear materials, they induce certain defects in the material such as vacancy or interstitial. These point defects lead to decrease in the strength of the material due to the microstructural changes taking place at the atomic level. Even though the time frame required to induce the micro-structural changes in nuclear materials takes time of weeks to years, the primary irradiation damage events leading to such microstructural changes last only for couple of picoseconds. There are several limitations associated with the experimental techniques to study these irradiation effects such as time, cost and even hostile environmental conditions. In such cases, computational approach becomes the only way to handle materials undeostile and extreme conditions that can never be

reached in a laboratory having high pressures and temperatures, presence of toxic substances or nuclear radiation. So, currently researchers are widely using the computational techniques to investigate such problems. Molecular Dynamics (MD) based atomistic modelling is one such computational method being used now-a-days on a wide scale to investigate irradiation induced micro structural changes at such short spatial and time scales. Such MD based simulations have been used by scientists to examine the effect of radiation damage on materials like Iron, Copper, Zirconium etc.

1.1 Concept of radiation damage:

Radiation damage is associated with ionizing radiation, which tends to be increasingly damaging in following order of molecular formation:

- Metallic bond (least damaged)
- Ionic bond
- Covalent bond (most damaged)

It is a significant contemplation while designing nuclear reactors (where radiation levels are pretty high), and also is one of distressing effects of nuclear weapons.

One of the major consequences of interaction of high energy particles (electrons, neutrons, ions and photons) with crystalline materials is creation of lattice defects. Figure 1, shows damage creation procedure in a displacement cascade activated by an anion or a neutron. The damage (along its evolution with time) governs macroscopic response of material to radiation, and hence is important to apprehend. Broadly, damage production can be divided into two categories: primary damage that is formed instantly after neutron/ion/electron impact by atomic collision processes far from thermodynamic equilibrium, and long-time scale (nanoseconds to years) damage evolution caused by thermally activated processes. The damage creation and its evolution with time as shown in figure.1 can be elucidated as follows:

1. High energy particle incident on the surface and interacting with the lattice atom.
2. The kinetic energy is transferred to lattice atom and it generates a PKA (primary knock-on atom).
3. Displacement of atom from its lattice position.

4. This PKA collides with other atoms in the lattice and it leads to the generation of additional knock-on atoms and further a displacement cascade is formed.
5. The relaxation phase in which several atoms with very high energy return to their lattice positions due to instability. In this phase, a high energy region is formed known as thermal spike.
6. Some atoms get permanently displaced from their lattice sites, leading to the generation of defects.

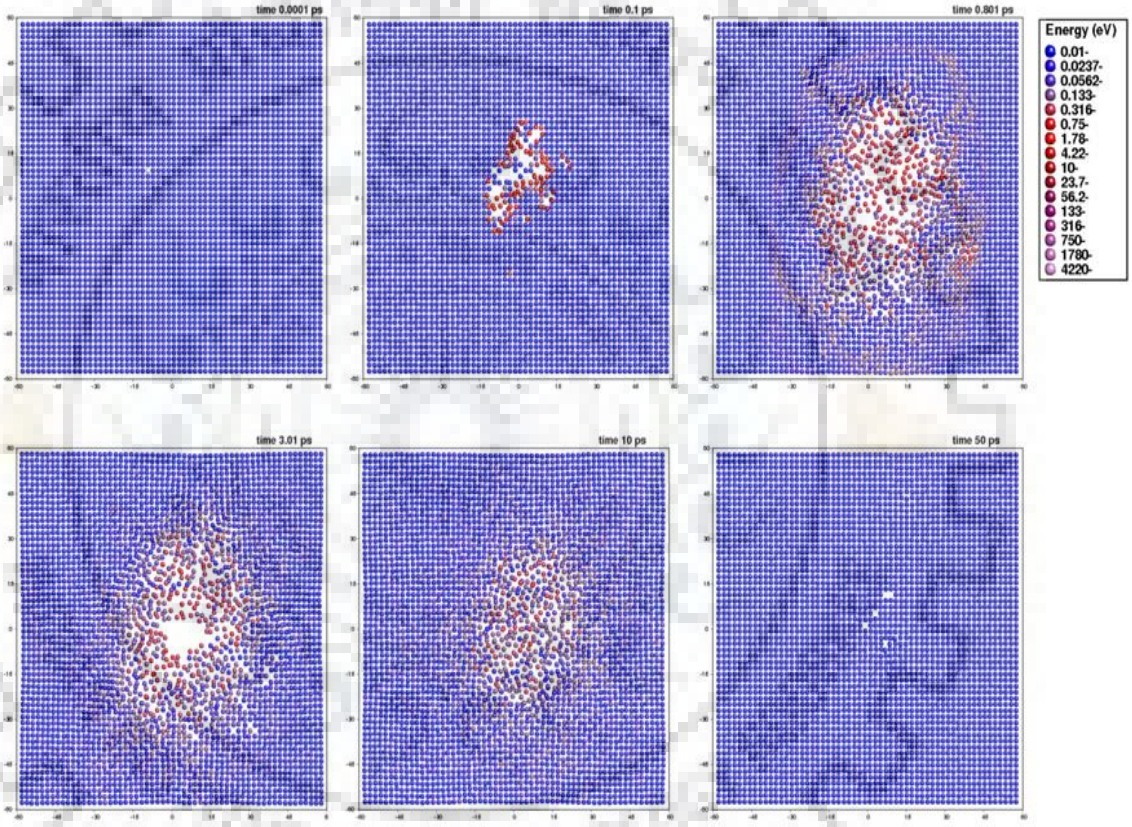

Figure 1: Evolution of displacement cascade over time. [1]

1.2 Displacement Cascade:

The displacement cascade in a solid (inside a solid structure) occurs when an atom in material is displaced from its site by an incident damaging particle and moves throughout material domain producing surplus displacements. It is used either to calculate an exposure parameter such as displacements per atom (dpa) as a method of comparing diverse irradiations and as a radiation induced defect source term in modelling effect of radiation.

Whenever a high energy particle (like neutron) hits an atom, it imparts a part of its energy to this atom, displacing it from its lattice site. Such an atom is known as PKA (this being the initiation stage). This particle further collides with other atom, transferring a part of its energy and so on. A lot of atoms have been displaced from their respective lattice site and the energy of the system increases. This shown by the second stage, i.e., the thermal spike. After this stage, the atoms start to lose relax and return back to their original site. This is relaxation stage. After this stage, only the stable defects remain in the cascade. These defects called as primary defects are the self-interstitial atoms (SIAs) and the vacancies. These form a Frenkel pair. When there is no dislocation or grain boundary present in the system, like in case of a single crystal the number of SIAs will be equal to the number of vacancies.

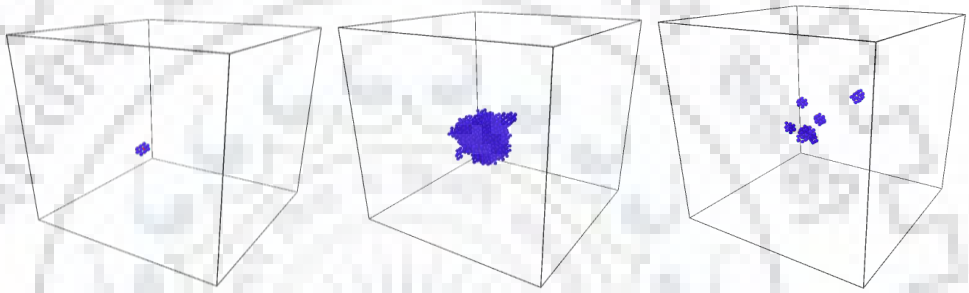

(a) (b) (c)

Figure 2: Three stages of a displacement cascade (a) Initiation (b) thermal spike (c) relaxation. [1]

Initiation phase: In the initiation phase of the displacement cascade, a high energy particle strikes the surface of the material and penetrates a significant distance through it before displacing the target atom from its lattice position. The target atom which is displaced from the lattice site due to the transfer of energy from the high energy particle is known as PKA.

Thermal spike: This is the second stage following the initiation phase. In this phase the PKA collides with the other atoms in the material and a cascade is formed. The cascade energy gets distributed among the atoms in that region. Thus, a hot region is formed in the material that is called as thermal spike.

Relaxation: In this last phase after the thermal spike, certain displaced atoms with the very high energy get back to their original lattice positions i.e. a process of recombination of

vacancies and interstitials takes place. Thus, this region is also known as the thermal spike cooling phase and it lasts only for few picoseconds.

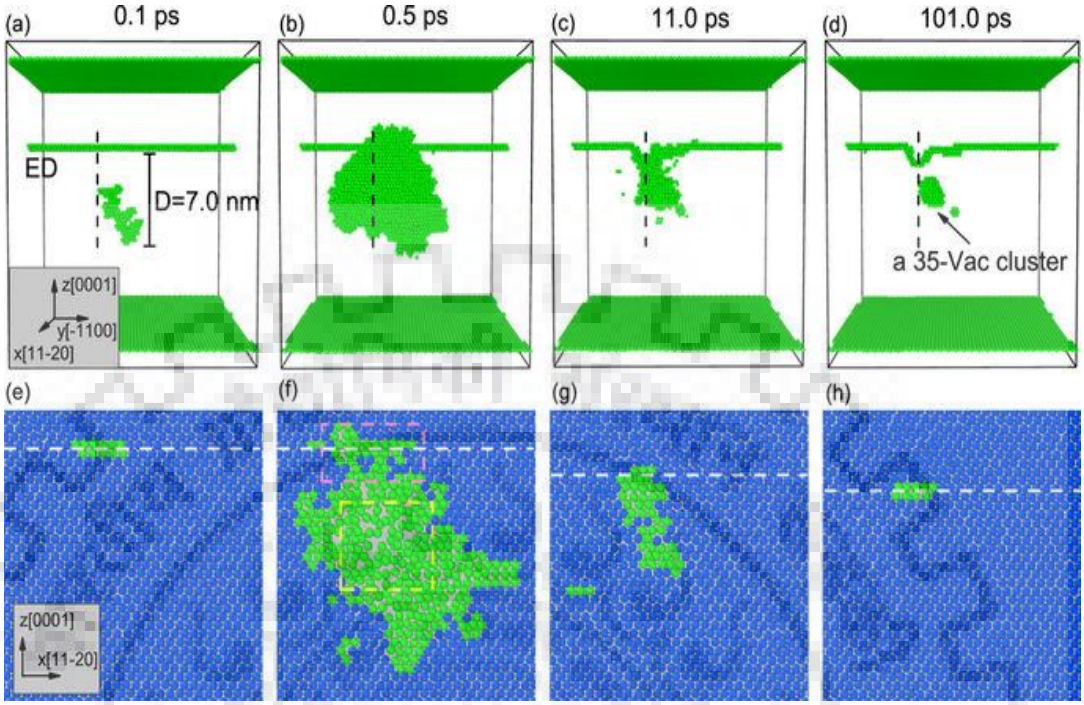

Figure 3: (a-d) shows the evolution of displacement cascade over time and (e-h) shows the rearrangement of atoms over different layers. [2]

The radiation has effects on the mechanical properties (including microstructural characteristics) includes changes in ductility and strength. Furthermore, the radiation can alter the electrical properties of material. Figure 3, also shows the process of initiation and evolution of displacement cascade over time along with how the atoms get re-arranged during this whole process over the different layers in the material.

MD based numerical simulations have comprehensively been employed by the scientists to explore the phenomenon of displacement cascades in metals such as iron [3], copper [4], tungsten [5] and Zr [6-7].

1.3 Characterizing Techniques:

The characterizing techniques may be either experimental or computational and have associated limitations with each of them. Computational techniques are considered less accurate as compared with experiments. Because experimental techniques involve large cost and time, and even some of them involve the hostile environmental conditions, that's why researchers are opting for atomistic simulation techniques to find new research directions.

There are various computational techniques which make use of FEM to investigate the defect generation and its effects, while some other methods make use of the classical mechanics. Generally, FEM based approach is used for the pure materials without any primary damage and the classical mechanics is employed for the damaged materials i.e. materials with defects like vacancy and interstitial. One such computational technique based on atomistic simulation called Molecular Dynamics (MD) is used for the materials involving the certain defects such as vacancy and interstitial.

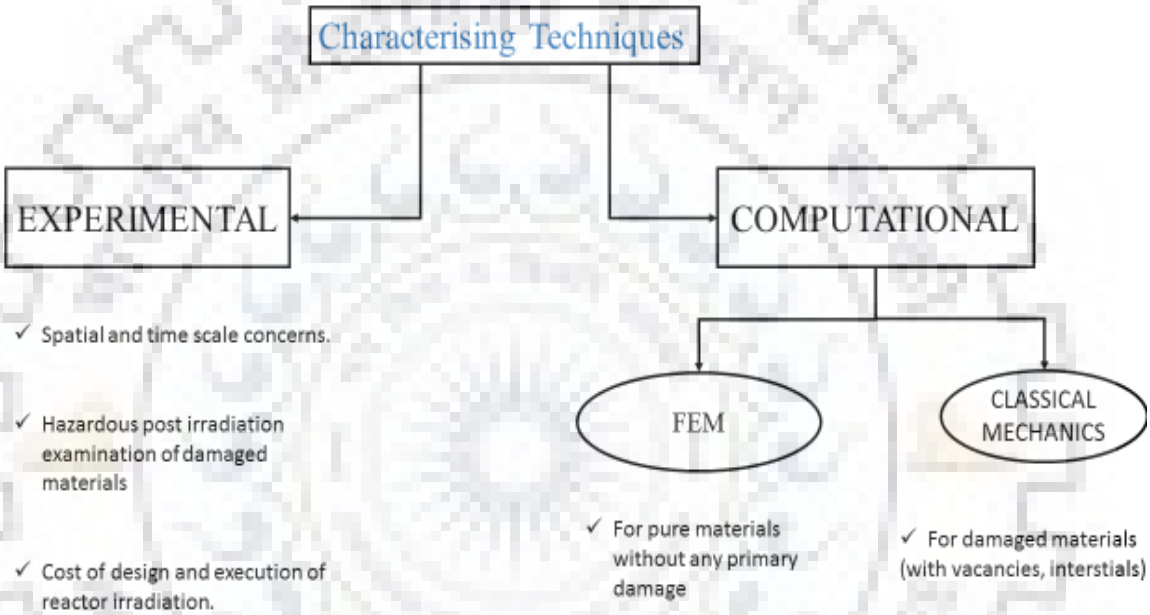

1.4 Modelling Techniques for Niobium:

There are various mathematical modelling techniques which have evolved in the last few years as an efficient tool to simulate the various problems and validate the theoretical results with the experimental results. These modelling techniques play an important role and are very effective in the study of various properties at the macroscopic level. These modelling techniques involve atomistic level modelling i.e. the main emphasis of the simulation work is at the atomic level. As a result, these techniques help us to analyse and understand the position and variation of each atom in the particular material. These modelling techniques can be classified as:

- Molecular Dynamics (MD)
- Molecular Mechanics (MM)
- Monte Carlo (MC)

1.4.1 Molecular Dynamics:

MD takes into consideration, the atoms as the basic interacting particles and neglects electrons or nuclei. As a result, the system can be well defined by using the Newton's equation of motion which involves the easy differential equations for atoms interaction only. Molecular Dynamics is a computer-based technique which involves the atomistic simulation of atoms or molecules (in the context of N-body systems). Molecular systems carry a large number of particles which makes it impossible to evaluate properties of such complex systems analytically; but MD circumvent this difficulty by using numerical methods. In MD, atoms are treated as classical particles. In these MD simulations, the atomic forces are calculated by utilising the atomic position and potential energy of system which is further used in Newton's equation of motion. The position, velocity and acceleration of each atom in system, is updated by using the relationship derived from Newton's motion equation at several time steps. Below mentioned equation is solved in various molecular dynamics based simulations:

$$m_\alpha \left(\frac{d^2 r}{dt^2} \right)_\alpha = -\frac{\partial U\left(r_1, r_2, ...r_N\right)}{\partial r_\alpha} = f_\alpha \qquad \alpha = 1, \ldots\ldots, N$$

Where, N is total number of atoms; m_α, r_α and F_α are mass, position and time dependent force acting on it due to external agents, respectively.

The potential energy 'E' is sub-divided into two parts i.e. internal part (E^{int}) and an external part (E^{ext}). The internal part describes the interaction between the atoms and the external part takes into account the constraints and the external fields.

MD simulations are carried out under diverse types of 'Ensembles' which is a collection of all possible different microstates of a system having an identical macroscopic state. Micro-canonical (NVE), canonical (NVT) and isobaric-isothermal (NPT) are the most frequently used ensembles.

MD simulation involves definition of a potential function (description of the terms by which particles in the simulation will interact). Mostly, the interatomic potentials employed in MD are either derived or developed empirically with help of higher fidelity numerical simulations or experiments. Interatomic potentials are mathematical expressions for estimating the potential energy of system of atoms. Frequently used interatomic potentials are empirical potentials, pair potentials versus many-body potentials, embedded atom method (EAM), semi-empirical potentials, polarizable potentials, etc.

Advantages of MD simulations:

- This method gives the better approximations to the results of the simulation as compared to the other methods like FEM etc. because it involves the computation at the atomic level and we very well know that the most of the system properties are dependent on the atomic arrangement in the structure.
- The values obtained after the computation are comparable with the experimentally obtained values.
- This method involves the use of only one mathematical equation i.e. the Newton's second law of motion, F = ma, and using this equation all the results of computation can be derived.

Limitations of MD simulations:

- The potentials used during the simulation are very limited and generally need to be driven empirically for multicomponent systems.
- Electromagnetic properties still cannot be obtained using the MD simulations.

1.4.2 Molecular Mechanics (MM):

This mathematical modelling technique makes use of classical mechanics to model the molecular systems. This technique can be used to study the molecular systems ranging in size from the very small to large material assemblies involving thousand to millions of atoms. Molecular mechanics have several areas of application, like in the field of Molecular

Dynamics, it uses the force field to calculate the force on the different atoms and also for modelling of particle or system dynamics and predict their trajectories.

1.4.3 Monte Carlo (MC) method:

This method of computation involves various computational algorithms which make the use of stochastic sampling of the data to obtain the results of the system. MC method are mostly used for probability distribution questions, optimization problems and numerical integration problems. In the industrial problems like failure prediction, cost estimation etc., this method proves to better than the other soft methods. This method finds the application in various other fields like physical sciences, engineering, computational biology, computer graphics, applied statistics, artificial intelligence, design and visuals, law, finance and business etc.

1.5 Interatomic potential:

Interatomic potential is a potential function which is used to describe the interaction between the particles and simulate them. These interatomic potentials are developed empirically by using numerical simulations or experimentally. There are various types of potentials used in the MD simulations as:

- Embedded atom method (EAM) potential
- Empirical potentials
- Pair potentials & many-body potentials
- Semi-empirical potentials
- Polarizable potentials etc.

1.5.1 Pair potentials:

In a system consisting of N number of atoms, an atom *i* interacts with all other atoms at same time (i.e. there are interactions of two-atoms, three-atoms, and so forth at any instant).

$$U = \sum_{i<j}^{N} U_2\left(r_i, r_j\right) + \sum_{i<j<k}^{N} U_3\left(r_i, r_j, r_k\right) + \cdots \ldots \ldots \qquad [8]$$

Pair potentials are simplest form of a potential that considers only these two-atom interactions and neglects all others. A typical example is the Lennard−Jones potential (Lennard−Jones 1924), U_{lj} (r), expressed in terms of interatomic distance, r.

1.5.2 Tersoff potential:

This potential is used for the covalent solids, which are less closely packed and have very strong directional bonds. For example, diamond and zincblende structures have a bond angle of ~109.47° and bonds of the hybridisation sp^3 . The general form of the Tersoff potential is:

$$U_{Tersoff} = \frac{1}{2} \sum_{i \neq j} U_R\left(r_{ij}\right) + \frac{1}{2} \sum_{i \neq j} B_{ij}\, U_A\left(r_{ij}\right) \qquad [8]$$

where, U_R and U_A represent repulsive and attractive potentials and B_{ij} is bond order between atoms i and j. The bond order for the bond between two atoms is a decreasing function of co-ordination number, N_{coor} .

$$B_{ij}\, \alpha\, \frac{1}{\sqrt{\mathrm{Ncoor}}} \qquad [8]$$

1.5.3 EAM potential:

EAM potential is an approximation relating energy between atoms and interatomic potential. The energy is a function of a sum of functions of separation between an atom and its neighbours.

Potential employed to represent the atomic interaction is whole solely responsible for the accuracy of the MD based simulation. The force matched (EAM) potential proposed by Fellinger et al. [9] has been utilized in this scrutiny. EAM potential has been well-established for use in atomistic simulations of metals and alloys. This potential consists of two terms: a many body term representing interaction between atom and electron cloud of surrounding atoms, and a pair wise interaction term representing the interaction between atom and its neighbours (see equation 1 for mathematical representation): [10]

$$E = \sum_i F_i(n_i) + \sum_{i<j} \emptyset_{ij}\left(r_{ij}\right) \qquad (1)$$

Here, E is overall potential energy of an atom, n_i is electron density, F_i is embedding energy and $Ø_{ij}$ is component representing pair wise interaction. In EAM potential proposed in the thesis, three functional forms (F_i, n_i and $Ø_{ij}$) were estimated by using the density functional theory, in which parameters were optimised to a well converged set of forces, stresses and energies. These models prove to be the promising candidate for metallic systems. EAM are widely used in MD simulations.

At higher energies, columbic interaction also become dominant. Modification is done in equation of EAM potential for accounting strong repulsive interaction, which not represented by EAM that would occur as a result of close approach between atoms.

Researchers have extensively employed the simulations of molecular dynamics to study various phenomenon occurring in the different materials at the micro structural level. In molecular dynamics we have to empirically generate interacting potential between the atoms. This potential is totally responsible for the results obtained for potential energy, forces etc.

Several researches have been made till now using the molecular dynamics-based simulations to investigate various properties of different elements like Zr, Fe, W, etc. Various researches in the field of nuclear industries which were carried out previously by the researches using the molecular dynamics-based simulations have given remarkable outputs which are in accordance with the experimental results.

1.5.4 Empirical potential:

The empirical potential are generally the force fields in the chemistry, while these are called the interatomic potentials in the materials physics. The force field in chemistry commonly employ the bonding interaction between the atoms to find out the energy of the bonded interaction and is not used for the modelling of the bond breaking and reactions explicitly. These potentials represent the quantum mechanical effects and they also contain certain free parameters like atomic radius, elastic constants, lattice parameters etc.

1.5.5 Semi-empirical potential:

The semi-empirical potential involves the use of the matrix representation in the quantum mechanics. Values of matrix elements are calculated with the help of the empirical formulae to

evaluate degree of overlap of the atomic orbitals. Further, diagonalization of the matrix is done to find out occupancy of different atomic orbitals. The energy contribution made by the orbitals is also calculated using the empirical formulae only.

1.6 Ensemble:

An ensemble is a collection of all possible microstates of the system, in which each atom moves and behaves differently but still have the same macroscopic or thermodynamic properties. So, in a MD simulation, we get a large set of atomic configurations which together makes an ensemble.

1.6.1 Types of ensembles:

The table shows the various types of ensembles used in the MD simulations with different fixed variables:

Table 1: Various ensembles used in MD and MC. [8]

Ensembles	Fixed variables	Remarks
Microcanonical	N, V, E	Isolated system Very common in MD $S = k \ln \Omega_{NVE}$
Canonical	N, V, T	Very common in MC Common in MD $F = -k\,T \ln \Omega_{NVT}$
Isobaric-isothermal	N, P, T	$G = -kT \ln \Omega_{NPT}$
Grand canonical	μ, V, T	Rarely in MD, more in MC $\mu = -kT \ln \Omega_{NPT}/N$

- **Microcanonical ensemble (NVE):**

  In microcanonical ensemble, the number of moles (N), volume (V), and energy (E) remains unchanged for the system. It resembles an adiabatic process and can be treated as an exchange between the kinetic and potential energy, while the total energy remains conserved. In a N particle system, having co-ordinates A and velocities V, the Newtonian expressions of the following first order differential equation will be; [11]

$$F(A) = -\nabla U(A) = M\dot{V}(t)$$

$$V(t) = \dot{A}(t)$$

The potential energy U(A) is the function of the particle co-ordinates A.

- **Canonical ensemble (NVT):**

  In this ensemble, the number of moles (N), volume (V), and temperature (T) does not vary for the system. In this ensemble a thermostat is used to exchange the energy between the endothermic and exothermic processes. This ensemble is also called the constant temperature molecular dynamics (CTMD) ensemble. [11] There are various methods to control the temperature like velocity rescaling, Berendsen thermostat, etc. Here, in this work the Nose-Hoover thermostat is used to control temperature to a constant value.

- **Isobaric-Isothermal ensemble (NPT):**

  In NPT ensemble, as name suggests, the number of moles (N), pressure (P) and temperature (T) remains conserved for the system. This means that along with the temperature, the pressure is also controlled. To control the pressure a barostat is also used.

- **Grand canonical ensemble (μVT):**

  In this ensemble, volume (V), temperature (T) of the system remains unchanged, similar to the microcanonical ensemble except the amount of substance that may vary in this case different from the NVT ensemble.

1.7 Niobium: Properties and applications:

Niobium, earlier known to be columbium, is a chemical element with symbol Nb (earlier Cb) and atomic number 41. It is a grey, soft, crystalline, ductile transition metal. Presence of properties like high ductility, corrosion resistance, hardness and low nuclear cross section makes Nb an important constituent element of the nuclear industry. It has low density and high melting point temperature, it is widely used in the alloy making and high temperature applications.

\

Figure 4: Zirconium crystal bar, Niobium, Zr-Nb alloy tubes [12,13,14]

It is widely used as the structural material in the nuclear powerplants. For example, in the pressure tube cladding of the fuel rods etc. It is also used with Zr to enhance its properties like high temperature stability, corrosion resistance etc.

1.7.1 Properties:

The various properties of Nb which makes it of great use in the various fields are: [15]

Poisson's ratio (μ)	0.4
Thermal conductivity (ρ)	53.7 $Wm^{-1}K^{-1}$
Bulk modulus (K)	170 GPa
Shear modulus (G)	38 GPa
Young's modulus (E)	105 GPa
Melting point temperature	2468^{o} C

Some other properties of Nb which were estimated with the help of the Molecular dynamics and validated with the experimental values are as follows: [15]

Lattice constant	3.308 Å
Cohesive energy	7.09 eV/atom

1.7.2 Applications:

Nb is an important constituent element of the nuclear industry and it has a number of applications both in elemental form as well as alloys. It enhances the properties of the other

nuclear materials when combined in an appropriate amount. Some of the important applications of the Nb are as follows:

1. Niobium is an important alloying element for steel, with which it forms niobium carbide and niobium nitride. These compounds increase grain refining, and retard recrystallization and precipitation hardening. [15]

Figure 5: Rods of steel-niobium alloy. [26]

2. Due to its high melting point temperature, Nb based alloys are widely used in the high temperature applications like fuel rod cladding in nuclear powerplants.

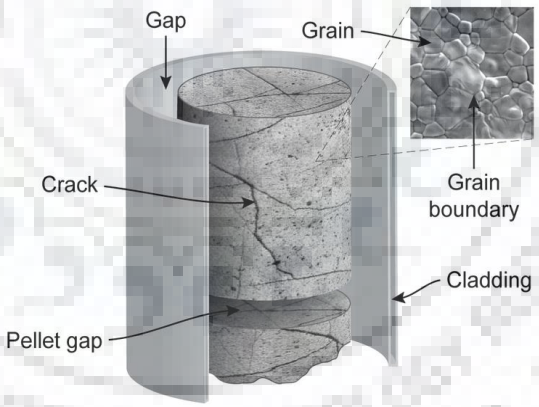

Figure 6: Fuel-rod cladding in nuclear powerplants. [27]

3. Apart from the nuclear industry, the Nb based alloys are also used in the aerospace industry such as jet engines and rockets.

Figure 7: Jet engine blades made of Nb based alloy. [28]

4. It is also used in the architectural designs such as beams and girders.
5. Due to its high pressure stability, Nb and its alloys also find application in the oil and gas pipelines, pressure tubes in the nuclear reactors.

Figure 8: High pressure tubes made up of Nb based alloy. [29]

6. In field of electronics, it acts as very important element for the superconducting materials, cell phones, pagers, laptops etc. It also has application in the optics, numismatics (making of coins) and design of jewellery.
7. "Gum metal" is an alloy of the Ti and substantial amount of the Nb and it possesses very unique deformation behaviour and remarkable properties. It is also called as multifunctional alloy due to its large number of application in aerospace industry, automobile parts, robot parts, sports equipments etc.
8. It primarily enhances the strength of the high-strength-low-alloy steels, when used as an alloying element.
9. It is also used in the automobile exhaust systems and Nb-Ti alloys which in turn are used to build the MRI (Magnetic Resonance Imaging) magnets.

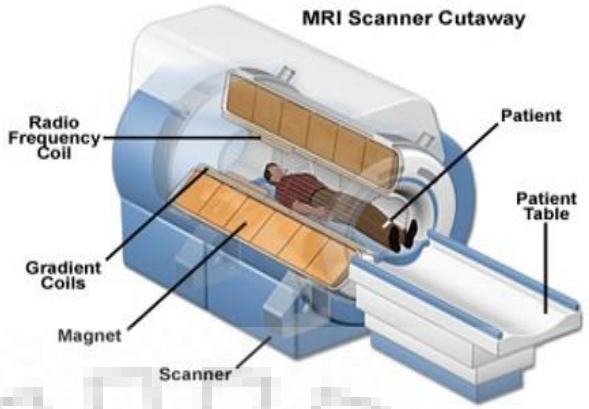

Figure 9: Magnetic Resonance Imaging machine. [30]

10. Nb is also mixed with the glass to get a higher refractive index value. This helps to obtain the thinner and lighter corrective glasses. [15]

1.8 Definition of problem:

Now-a-days the conventional energy resources are depleting day by day, so, there is a need for some unconventional energy resources like the nuclear materials. The use of these nuclear materials as a source of energy is still under research. These nuclear materials are also being used as the structural materials in the nuclear industries. During their operation, these materials are posed several radiation induced defects. It is of great necessity to study that how these defects and their distribution affect the properties of the nuclear material. Experimentally, it is very difficult to study these irradiation induced phenomenon due the hazardous environmental conditions in nuclear industries. So, in this dissertation work, efforts have been made to study these effects computationally by utilizing the MD based simulations.

1.9 Brief description of the work:

In this dissertation work, the main focus of discussion is the effect of the radiation damage in the Nb bi-crystal in conjunction with the asymmetric and symmetric tilt grain boundaries. Initially, for single crystal of Nb, generation of the crystal was done using the MD (Molecular Dynamics) modeling techniques and then the cohesive energy was calculated. Furthermore, the point defects (i.e. vacancy and interstitial) were generated in the crystal and their formation energies were estimated using MD. In case of the Nb bi-crystal, similar to the single crystal,

two such crystals were generated and they were oriented at various mis-orientation angles w.r.t. each other to generate the grain boundary. Further the grain boundary energies were calculated for the different grain boundary structures generated. After this, similar to the single crystal, the defect (vacancy) was generated in the bi-crystal, both in the bulk and near the grain boundary and their formation energies were calculated using the molecular dynamics simulations. The effect of these grain boundary structures was also studied on the defect formation and distribution. Previous researches have established that the GB structures act as the sink for the point defects. The eradication of the point defects by the grain boundary further prevents clustering of these defects, which in turn avoids unfavorable microstructural changes leading to the structural failures. The micro structure of these grain boundaries affects the defect formation and the energy required for their formation to a large extent.

In the further work of the dissertation, the vacancy migration and its energy calculation has been described by using the concept of NEB (Nudged Elastic Band), both for the STGB and ATGB structures. In this study, the vacancy migration was considered in the form of several replicas of the system which represent the various transition states. These transition states have an energy barrier and the maximum of these is called as the VME (vacancy migration energy).

CHAPTER 2
LITERATURE REVIEW

Niobium is an important constituent element of the nuclear industry as it is widely used as the structural material in various components of the nuclear reactor. It is widely used as an alloying element with Zirconium etc. to enhance its mechanical properties. Due to its wide applications in nuclear powerplants, there is a need to study the effects of the atomic structure on the radiation induced defects in bcc Nb. A number of studies have been made on the materials like Zirconium, Iron, etc. but there is a very few literature available regarding the work on Niobium.

The experimental work performed by Tucker et al in 1969, [16] describes the creation of dislocation channels in irradiated single crystal of Nb. These dislocation channels were created as a result of the plastic deformation following the irradiation, which made the pathways cleared of the defect clusters. In 2017, Avinash and Divya [10] performed studies about the impact on tensile strength of single crystal of Nb by irradiation phenomenon. Their work shows that the mechanical strength of Nb is governed to a large extent through the dislocation channeling and it was in accordance with experimental work performed by Tucker et al. [16].

Figure 10: Activated slip planes at onset of plasticity in simulations accomplished with diverse PKA energy level. [10]

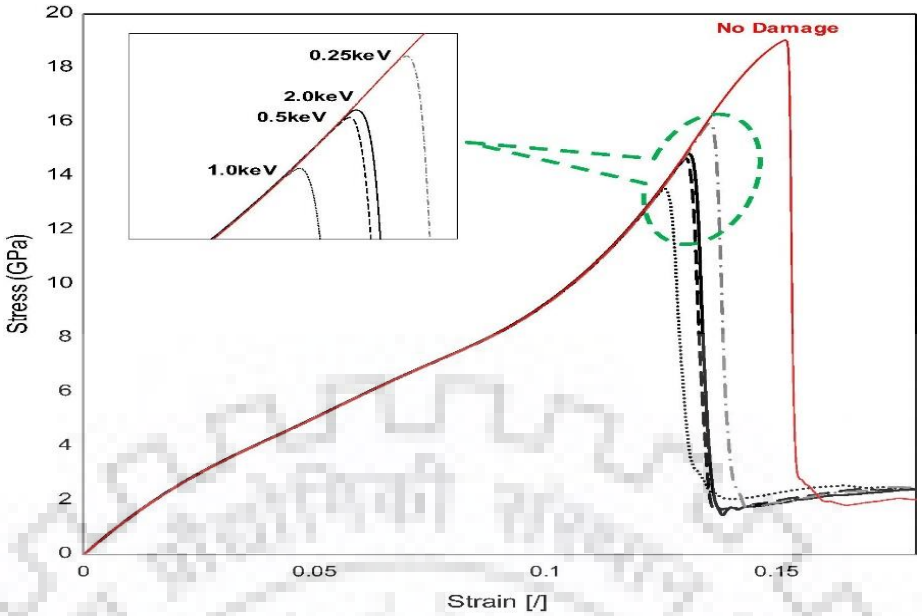

Figure 11: Stress-strain response captured with altered PKA energies at a temperature of 10 K. [10]

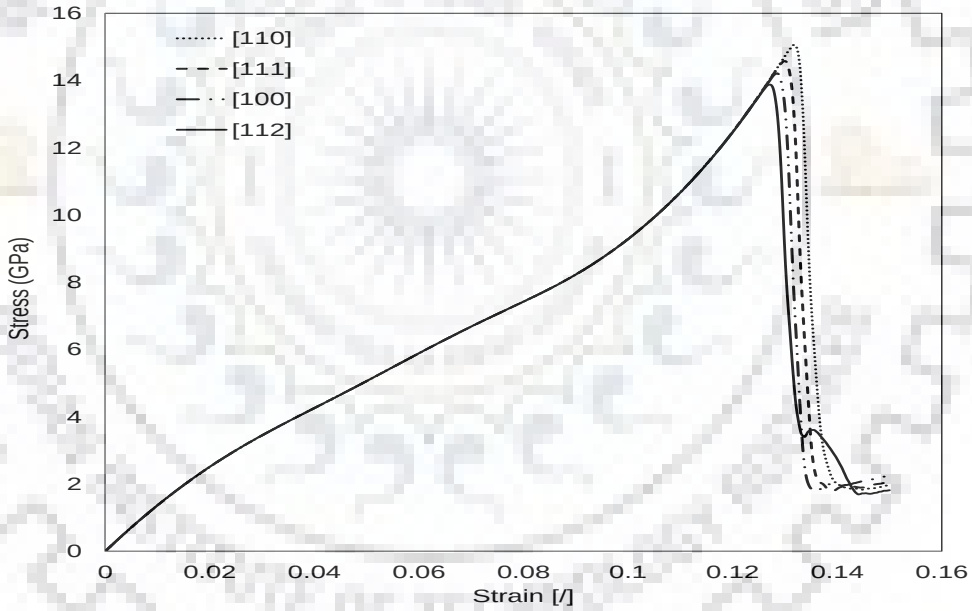

Figure 12: Stress-strain response captured with altered PKA velocity vectors at a temperature of 10 K. [10]

They, also discussed in their paper about the impact of temperature of the simulation box, primary knock-on atom (PKA) energy and primary knock-on atom (PKA) velocity vector on the number of Frenkel pairs generated. The plots (a) and (b) in the figure 8 and figure 9 respectively, represent the same. They also concluded that temperature heals the defects like (vacancy and interstitial) produced due to irradiation. The displaced atoms settle down back to their lattice positions due to this healing effect of the higher temperature.

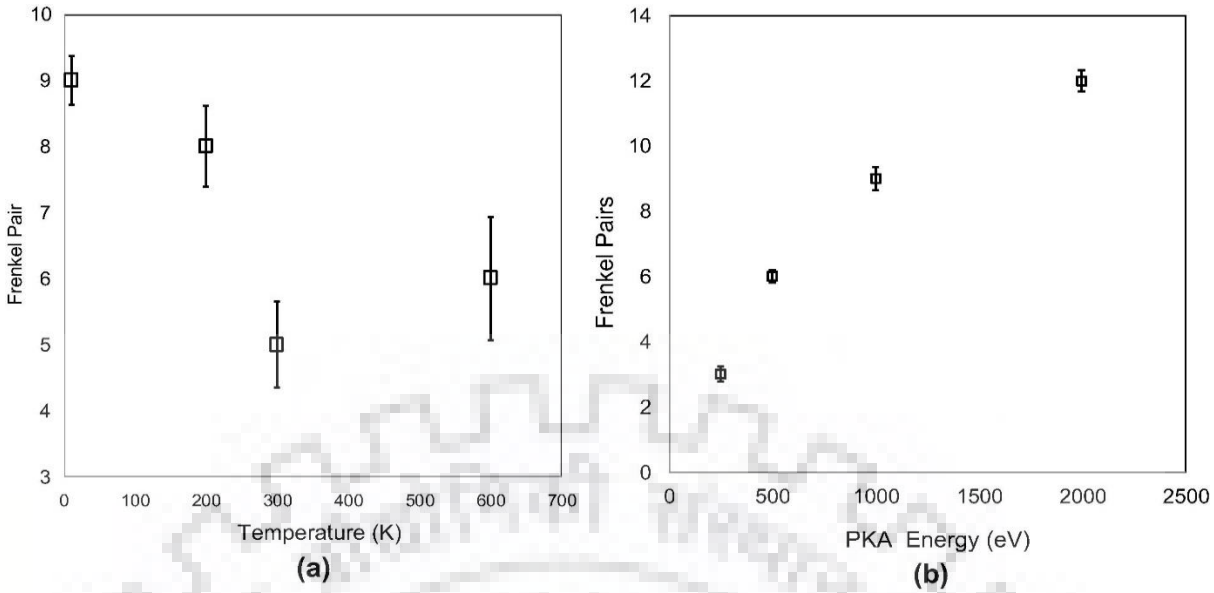

Figure 13: Frenkel pairs generated in MD based simulation with respect to (a) simulation box temperature, and (b) PKA energy. [10]

Figure 13(a), depicts that the temperature affects the number of defects very slightly at the equilibrium. At the initial lower temperature of 10^{o} K the number of defects are maximum, which decreases as the temperature of the simulation box increases to 600^{o} K and obtains a minimum level. In figure 13(b), there is a continuous rise in the number of defects with increasing PKA energy. For this case, in the distribution of the vacancy, there are formations of the small clusters of the vacancies, as compared to the vacancy distribution w.r.t. temperature.

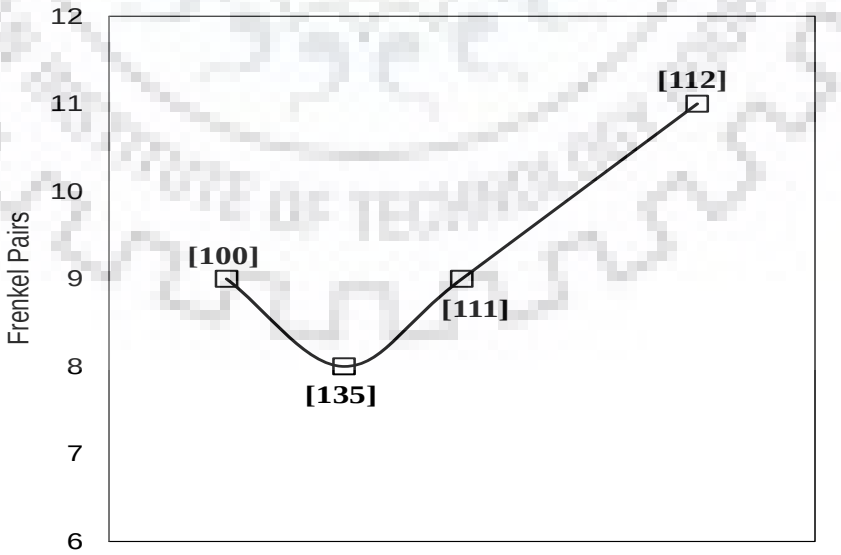

Figure 14: Frenkel pair generated with respect to PKA velocity vector aligned with various crystal orientation. [10]

From figure 14, we can clearly understand the variation of number of defects w.r.t. the PKA velocity vectors along with the lattice directions [100], [135], [111] and [112] respectively. The plot clearly depicts that, for the velocity vector aligned with lattice direction [112], the number of defects are maximum. This was attributed to the fact that in bcc-crystal <112> plane is a principle slip plane and thus increases the number of defects generated in a single crystal of Nb.

The defect distribution (i.e. vacancies and interstitials) was also studied in this chapter and it was concluded that the formation of vacancy was in small clusters and the interstitials were scattered as compared to the vacancy in the simulation box., w.r.t. each simulation box temperature, primary knock-on atom (PKA) energy and primary knock-on atom (PKA) velocity vector.

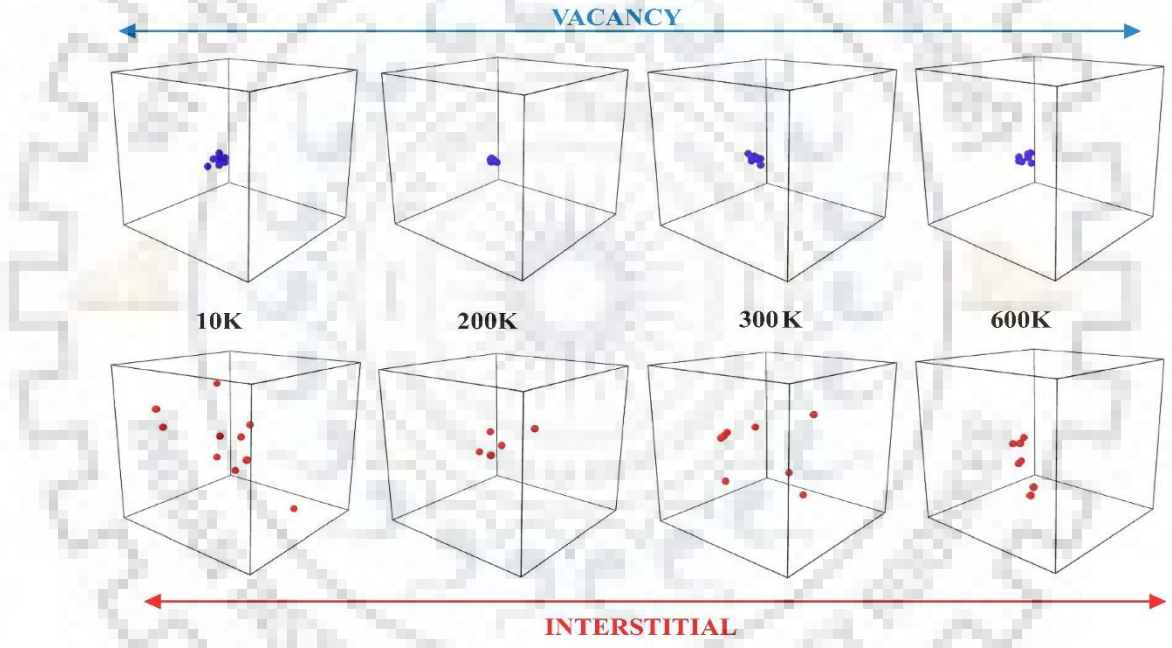

Figure 15: Distribution of vacancy (blue atoms) and interstitials (red atoms) in simulation box with respect to simulation box temperatures, PKA energy and PKA velocity vector. [10]

Their further work in 2017, [17] also explains the outcome of symmetrical and asymmetrical tilt GB on tensile behavior of bcc Nb. In this work, they studied the outcome of GB structure on mechanical response of the Nb bi-crystals. They concluded from their work that symmetrical GB have comparatively stable atomistic configuration and lower energy as compared to the asymmetrical tilt GBs.

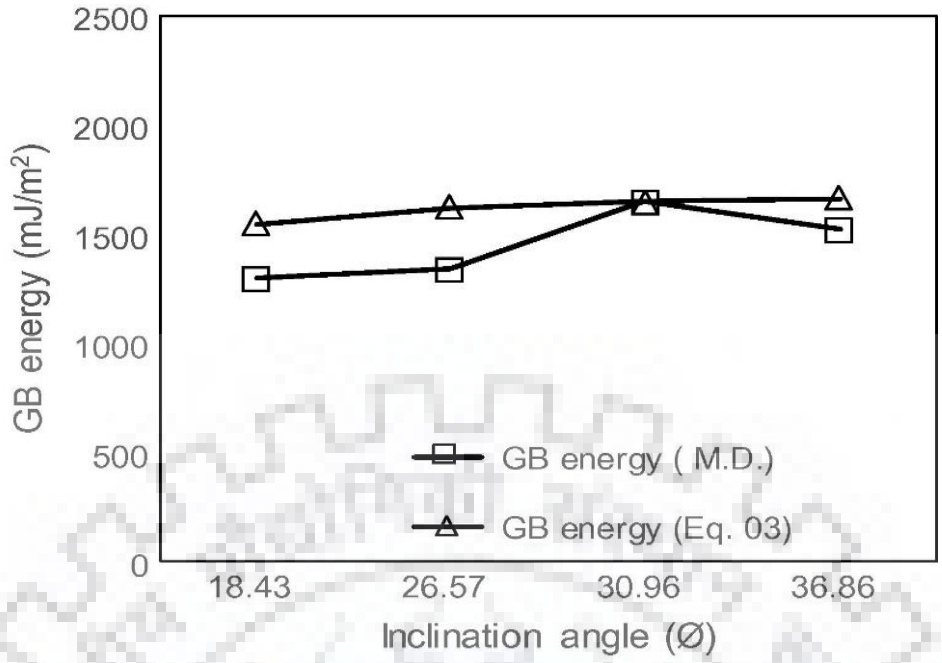

Figure 16: Asymmetrical tilt grain boundary energies at mis-orientation angle of 36.86^{o} as a function of inclination angle (Ø). [17]

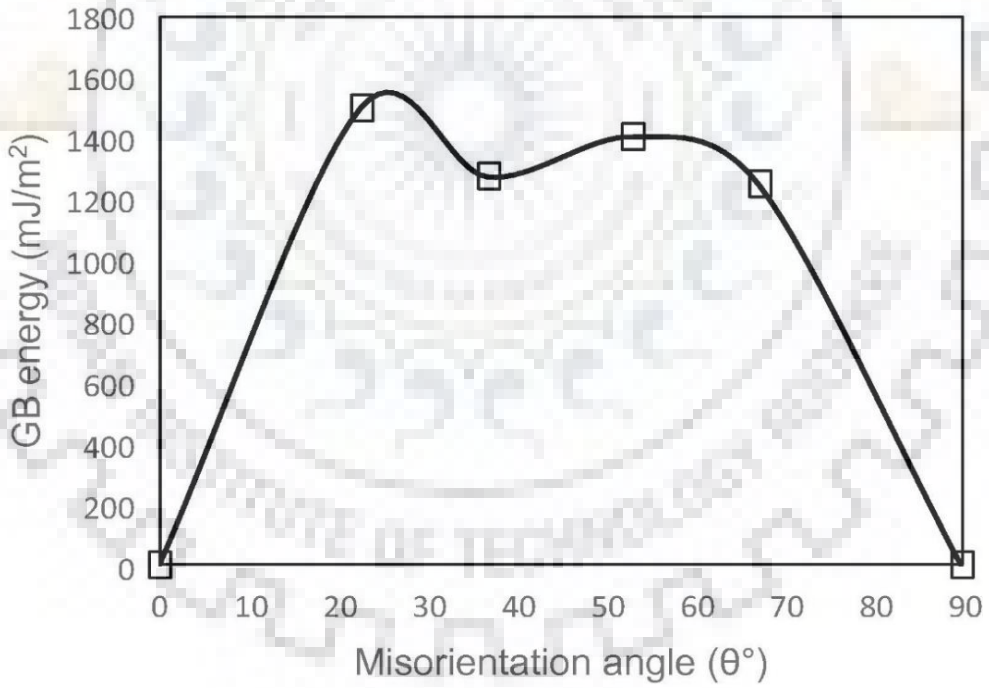

Figure 17: Deviation in GB energy with respect to mis-orientation angle along 〈1 0 0〉 tilt axis. [17]

They also concluded that as the mis-orientation angle increases, the yield strength of bi-crystal also increases.

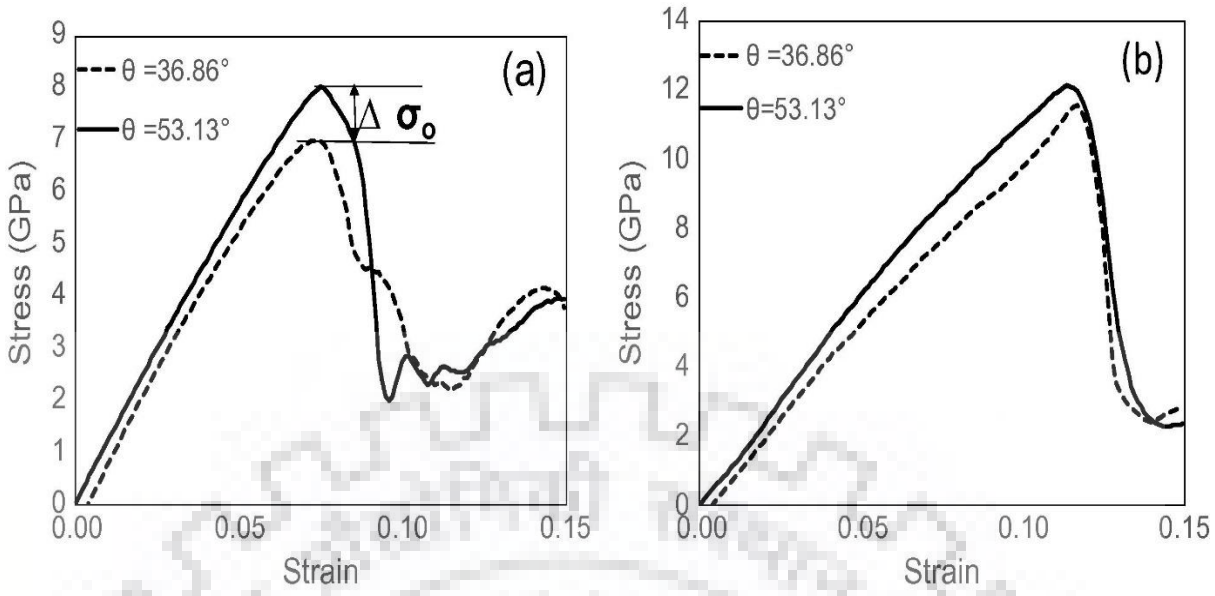

Figure 18: Stress-strain curve for 36.86° and 53.13° mis-orientation angle with 〈1 0 0〉 tilt axis at (a) 300 K, (b) 1 K. [17]

The deformation mechanism of the bi-crystal when it is subjected to the tensile loading, was also discussed in the paper, both for asymmetrical and symmetrical tilt GBs. Figures 19 and 20 are showing the dislocation nucleation and growth for STGB and ATGB structures at two different temperatures i.e. 1K and 300K.

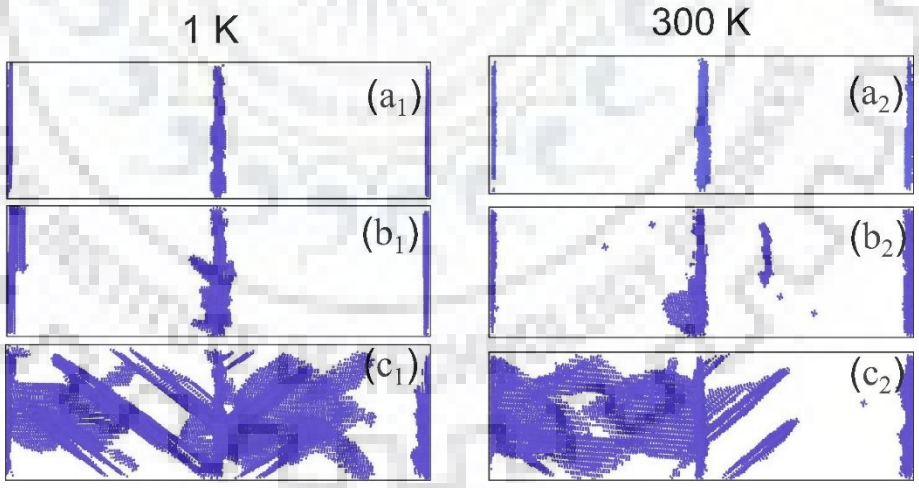

Figure 19: Dislocation nucleation and growth in STGB for θ = 36.86° mis-orientation angle at 1 K and 300 K (a_1, a_2) Before yield (b_1, b_2) At yield (c_1, c_2) After yield. [17]

In figure 19, the snapshots of simulation box shows processes of dislocation nucleation and growth in symmetrical tilt grain boundary (STGB) for the mis-orientation angle of θ = 36.86°. Common neighbour analysis (CNA) and Taylor's work hardening expression was utilised

during this study. CNA helps to identify the atoms not being in bcc lattice configuration, like atoms at grain boundary. Here, evolution of dislocation is shown at three different stages i.e. before, at and after yield. The density of dislocation nucleation is more for the simulation performed at the 1K as compared to 300K. This entanglement of dislocations leads to increase in the strength of the material.

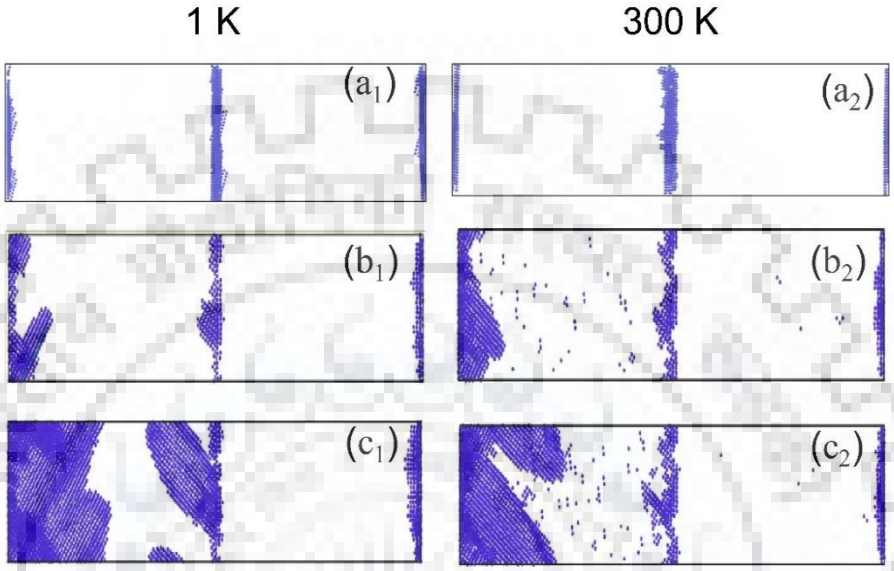

Figure 20: Dislocation nucleation and growth in ATGB for θ = 36.86° and Ø = 26.57° at 1 K and 300 K (a_1, a_2) Before yield (b_1, b_2) At yield (c_1, c_2) After yield. [17]

Similarly, the figure 15, shows the snapshots of simulation box representing dislocation nucleation and growth for the asymmetrical tilt grain boundary (ATGB) for inclination of Ø = 26.57°. Here, the distribution of the dislocation evolution is not symmetric about the grain boundary. On one side of the grain boundary the dislocation density is very high as compared to the other side, as can be seen in the figure 20 (c_1) and (c_2).

In 2008, Lewis with some other researchers performed the experimental studies on the polycrystalline Nb to investigate the effect of dislocations in which the quasi-static tensile loading was imposed on the polycrystalline Nb. [18]. In 1972, Szkopiak estimated the Hall-Petch parameters of Niobium like Hall-Petch constant 'K' and friction stress value using the extrapolation and grain size methods. [19]. In 2013, B. Joni et al. [20] studied the impact on mechanical properties of Nb due to dislocation density and grain size, by employing the X-Ray diffraction techniques.

When the nuclear materials are exposed to the radiation in the nuclear power plant, they develop certain point defects such as vacancies and interstitials, which are the results of the displacement cascades. In previous researches, it has been found and stated that grain boundaries act as the sink for such point defects (i.e. vacancies and interstitials). These extreme irradiation phenomena lead to the swelling, embrittlement, stress and corrosion cracking in the materials.

Recently in 2018, Divya and Avinash have considered the effect of symmetrical and asymmetrical tilt GB on the formation and spatial distribution of radiation-induced point defects in Zirconium (Zr). [21]. They determined from their work that grain boundary structures have a substantial influence on creation and dispersal of the radiation-induced point defects.

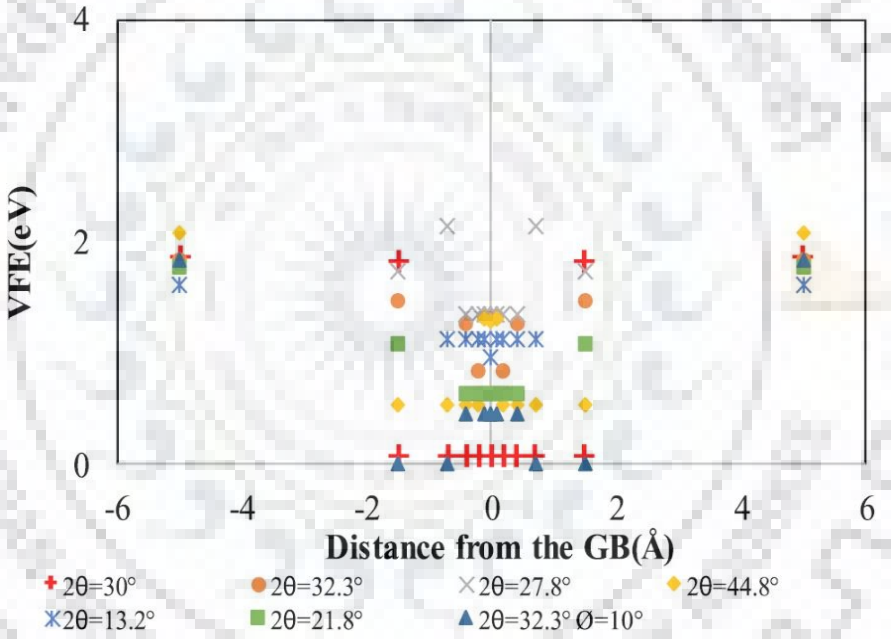

Figure 21: Variation in VFE as a function of misorientation angle, and the distance from GB for [0 0 0 1] as tilt axis. (The VFE for an asymmetrical GB (Ø = 10°) is also plotted.) [21]

From the figure 16, it was concluded that the value of vacancy formation energy (VFE) decreases as we approach the grain boundary and it is equal to zero at the grain boundary. This can be attributed to the fact that near the grain boundary the atomic structure is more incoherent as compared to the atomic structure away from the grain boundary. A similar variation for interstitial formation energy (IFE) was also obtained in the paper.

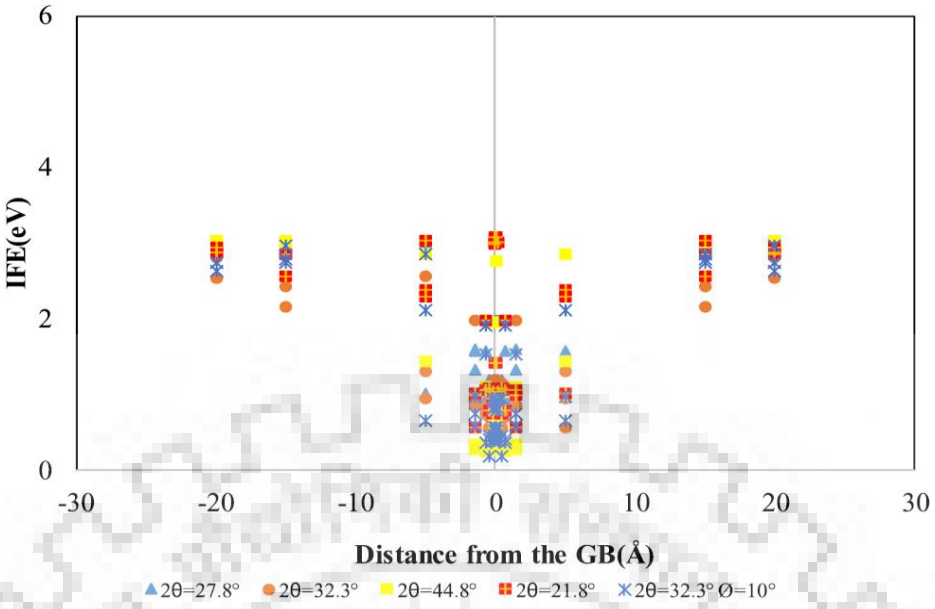

Figure 22: The variation in IFE as a function of misorientation angle and distance from GB for [0 0 0 1] as tilt axis. (IFE for an asymmetrical GB (Ø = 10°) is also graphed.)[21]

They also concluded that the point defect formation energies (i.e. VFE and IFE) does not depend directly on the mis-orientation angle, but largely depend on the grain boundary energies. The VFE and interstitial formation energy (IFE) with higher energy grain boundary structures have lower values as related to the grain boundaries having the lower energies.

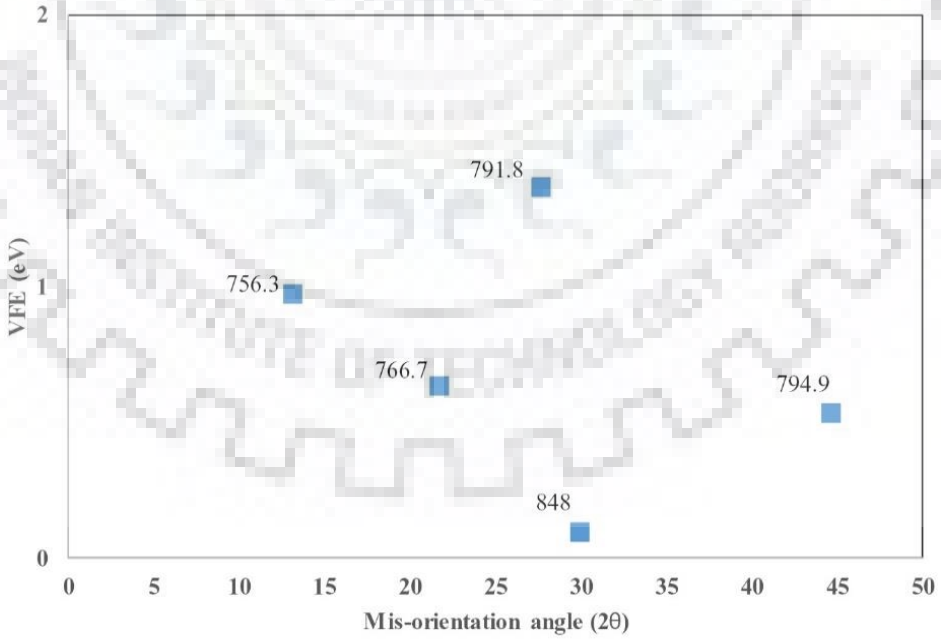

Figure 23: The trend of VFE as a function of misorientation angle along tilt axes aligned with [0 0 0 1]. The values specified next to data points correspond to the GB energies at specific misorientation angle. [21]

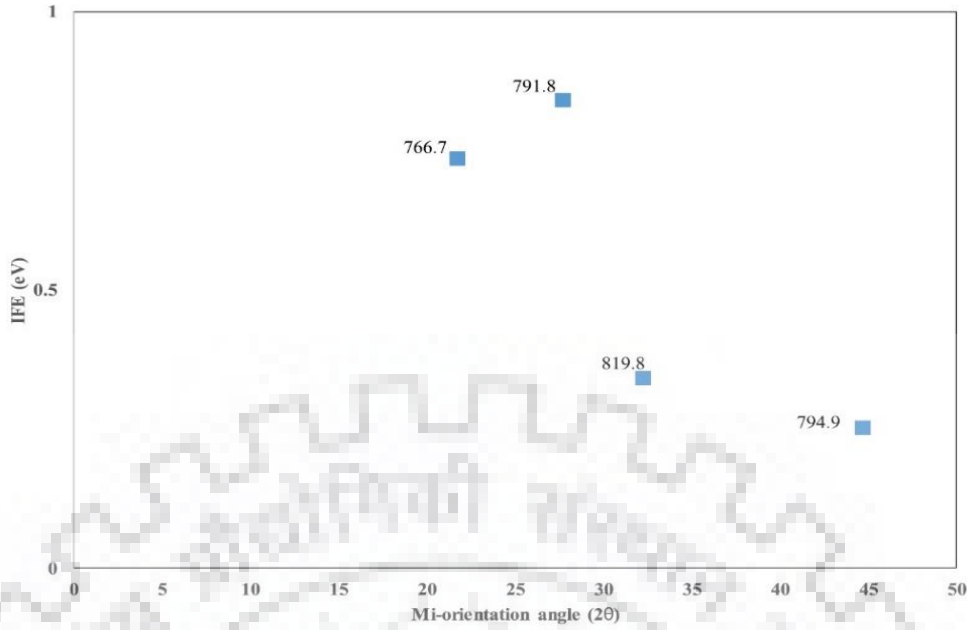

Figure 24: The trend of the IFE as a function of misorientation angle along the tilt axes aligned with [0 0 0 1]. The values specified next to data points correspond to GB energies at certain misorientation angle. [21]

The figure 18 and 19, in their work represent the trend of the VFE and IFE with respect to the mis-orientation angle. The plots show that there is no particular trend of the variation of VFE and IFE w.r.t. mis-orientation angle.

Some other works on MD based simulations, so far:

1. **Rajesh Kumar and Avinash Parashar (2015):** In this paper the MD based atomistic simulations were accomplished to examine the failure or fracture mechanism of the BN nanofillers for the mechanical properties.

2. **G Rajasekaran, Rajesh Kumar and Avinash Parashar (2016):** This article focuses on the MD based stomistic simulations performed to improve accuracy of the Tersoff potential. This helps to simulate the graphene in the MD environment. An interatomic potential with some modification in the cut-off function for the Tersoff potential was defined for the single sheet of graphene to predict its realistic behavior.

3. **G Rajasekaran and Avinash Parashar (2016):** In this article, mechanical response and failure behavior of the graphene is described. This describes the geometry dependency of the mechanical properties and failure behavior of graphene. The author also suggests the 5-7-7-5 (pentagon-heptagon-heptagon-pentagon) structure for the performance enhancement. Their work suggests that with some modification in the structure of graphene sheet, (like creating defects), there is enhancement in the electrical and mechanical properties, as well as some new functionalities are also developed, which are not found in the pristine graphene.

4. **Rajesh Kumar and Avinash Parashar (2017):** In this article atomistic simulations were performed to find out the effect on the mode-I fracture toughness of the h-BN nanosheets assisted with the dislocations. Different geometrical configurations of the dislocation were used during the molecular dynamics-based simulations with a central crack in the sheet. The dislocation assisted crack healing phenomenon was also observed during the simulations.

5. **Divya Singh, Avinash Parashar, Rajeev Kapoor, Apu Sarkar, A. Kedharnath (2019):** In this article, the studies were made on the effect of symmetrical and asymmetrical tilt grain boundaries on the tensile deformation of the Zirconium bi-crystal. To generate the tilt grain boundaries about the [0001] as the tilt axis, molecular statics-based simulations were employed and to further study the effect of radiation induced point defects w.r.t. deformation behavior and effect on grain grain boundary structure, molecular dynamics-based simulations were used. They concluded from their simulations that the main mechanisms leading to deformation were twinning, shift in grain boundaries and formation of dislocation networks. Finally, the authors concluded that the grain boundary structures are mainly responsible for the deformation behavior of the bi-crystalline Zirconium.

6. **Buchler et al. (2002):** In this article, the author made the study to investigate the ductile material failure using MD simulations. For the study, the author incorporated a huge number of atoms in a simulation box.

7. **Namilae et al. (2002):** MD simulations were used by the authors to investigate the grain boundary formation and sliding in the bi-crystal of Aluminium (i.e. symmetric tilt boundaries of Al and Mg doped Al).

8. **Zheng and Zhang (2006):** In this article, the mechanical deformation behavior of the nano-crystalline copper was studied using the molecular dynamics-based simulations.

So far, the literature related to the grain boundary generation, estimation of the corresponding grain boundary energies and defect formation energies (VFE and IFE) and defect migration energies (VME) in bi-crystals of Niobium with tilt axis aligned along the [0001] axis has been almost non-existent. So, in this dissertation work, an attempt is made to study these defect formations in the Nb bi-crystal, both with the symmetrical and asymmetrical grain boundaries for tilt axis aligned with [0001]. The results of the energies are tabulated and plotted in the chapter 4 of the report.

CHAPTER 3

MODELLING DETAILS

In the present work, the MD based calculations were performed in the Large Scale Atomic/Molecular Massively Parallel Simulator (LAMMPS) and further analysis of the dump files was done in Open Visualization Tool (OVITO). Potential used for assessing the interatomic forces totally governs the reliability and accuracy of any MD simulation. So, Embedded Atom Method (EAM) potential suggested by Fellinger for Nb [9] was used in all the simulations done during this work.

3.1 Single crystal of Nb:

Initially, for the single crystal of Nb, the crystal was generated using the atomistic modeling. In this a simulation box was created by providing the dimensions and the boundary conditions (BC) were imposed on simulation box. Periodic boundary conditions were imposed to avoid any edge effect. This simulation box resembles the single crystal of Niobium. Further, the interatomic potential was defined for the atomic interactions, using which the total potential energy of system was calculated. Thereafter, cohesive energy (E_{coh}) was calculated for the Nb crystal by dividing the total potential energy by total number of atoms in Nb crystal. In the further simulation work vacancy was created in the Nb crystal by deleting an atom and then the system was minimized to obtain the minimum energy crystal structure. The vacancy formation energy was then calculated using the equation

$$E_{vac} = E_f - E_i + E_{coh} \qquad (2)$$

here, E_{vac} = vacancy formation energy, E_f = energy of the system after the formation of vacancy, E_i = energy of the system before the formation of vacancy, E_{coh} = system's cohesive energy

Similarly, IFE was also estimated, with the difference that inplace of deleting, an extra atom was included to the Nb crystal. The IFE for each configuration was estimated by using the following equation:

$$E_{int} = E_f - E_i - E_{coh} \qquad (3)$$

3.2 Nb bi-crystal simulations:

In this work, for Nb bi-crystal simulations were executed in the two stages. In initial stage, asymmetrical tilt grain boundaries (ATGB) and symmetrical tilt grain boundaries (STGB) were produced along [0001] as the tilt axis and their corresponding GB energies were calculated. The set of grain boundaries generated consists of 9 STGB and 5 ATGB along the [0001]. The modelling details of the GBs are provided in the tables 2 and 3, for STGB and ATGB respectively. Periodic boundary conditions were imposed on all the boundaries of simulation box, to avoid edge effects. In order to circumvent any sort of image interaction between grain boundaries, size of simulation box was kept large enough. GB planes for both the crystals remain same in STGB while they differ in case of the ATGB. In this whole article, the misorientation angle and the inclination angle is represented with '2θ' and 'θ' respectively.

Firstly, the symmetrical tilt grain boundary (STGB) was created by rotating lower half and upper half of Nb bi-crystal in the clockwise and anti-clockwise directions respectively about [0001] tilt axis with an angle of rotation equal to tilt angle. The overlapping atoms were then deleted by using the appropriate deletion criterion. Further, the GB structure was minimized by utilizing the conjugate gradient (CG) algorithm until steady state in system was achieved with minimum energy, at 0 K.

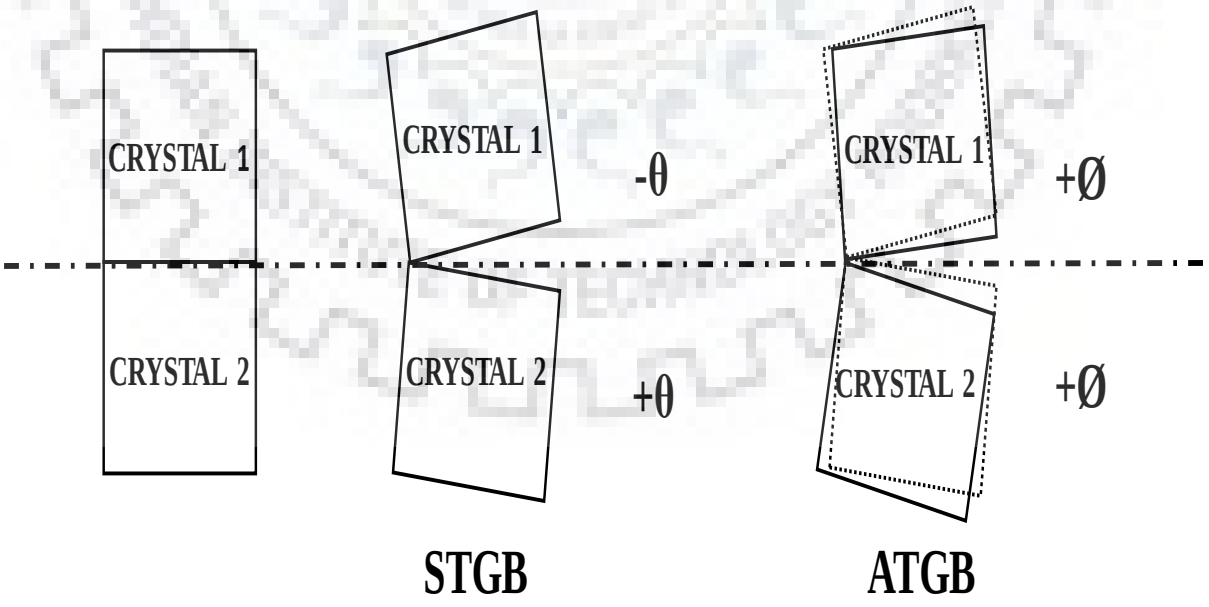

Figure 25: Diagram of generation of symmetric tilt grain boundaries (STGB) and asymmetric tilt grain boundaries (ATGB)

Table 2: Configuration particulars of STGB tilted along <0 0 1> axis.

S.No.	GB plane (hkl)	Mis-orientation angle (2θ)	Simulation box dimensions (Å)
1.	**(1 0 0)**	**0º**	**330.2 x 198.48 x 16.51**
2.	**(5 1 0)**	**22.61º**	**165.1 x 198.48 x 33.02**
3.	**(9 2 0)**	**25.06º**	**132.08 x 198.12 x 66.04**
4.	**(3 1 0)**	**36.86º**	**138.68 x 330.8 x 33.02**
5.	**(5 2 0)**	**43.6º**	**141.98 x 198.12 x 33.02**
6.	**(2 1 0)**	**53.13º**	**141.98 x 198.12 x 66.04**
7.	**(3 2 0)**	**67.38º**	**161.79 x 198.48 x 33.02**
8	**(4 3 0)**	**73.73º**	**330.2 x 198.12 x 33.02**
9.	**(1 1 0)**	**90º**	**330.2 x 198.48 x 16.51**

Table 3: Configuration details for ATGB tilted along <0 0 1> for 36.86º mis-orientation angle.

S.No.	Inclination angle (Ø)	GB plane(s) $(hkl)_1/(hkl)_2$	Simulation box dimensions (Å)
1.	**30.96**	**(6 7 0)/(9 2 0)**	**128.77 x 330.2 x 99.06**
2.	**33.69**	**(3 4 0)/(11 3 0)**	**181.61 x 330.2 x 66.04**
3.	**36.86**	**(5 7 0)/(3 1 0)**	**158.49 x 330.2 x 66.04**
4.	**43.6**	**(5 9 0)/(11 5 0)**	**181.61 x 330.8 x 66.04**
5.	**53.13**	**(1 3 0)/(7 5 0)**	**191.52 x 330.2 x 66.04**

In order to achieve the minimum energy GB structure, further volume relaxation perpendicular to the GB plane was performed. Several deletion criteria were used to obtain the stable grain boundary structure with the minimum energy and structure with most coherent configuration was then selected as final grain boundary. To calculate the GB energy, the following equation (4) was used: [21]

$$E_{GB} = (E_T - E_B)/(2 \times \text{Area}) \quad (4)$$

where, E_{GB} = GB energy, E_T = total minimum potential energy of system calculated through MD, E_B = total cohesive energy of system and Area = area of GB.

ATGBs were generated by rotating the lower and upper half of symmetric bi-crystals either in clockwise or anti-clockwise direction. This rotation of the two halves was performed with an angle equal to inclination angle. By doing so, asymmetry is introduced in the bi-crystal and the misorientation is also maintained. For ATGB, to get a perfect crystal we tune the simulation box with several number of iterations while it is comparatively easier to generate a STGB.

3.3 Defect generation and VFE calculation:

In the next stage, calculation of VFE and IFE was carried out for both STGB and ATGB developed along [0001] tilt axis. To calculate the (VFE), a vacancy was created in Nb bi-crystal by deleting an atom, one near the GB and another at some distance (i.e. in the bulk). Further, by using a CG algorithm, the system was relaxed and the energy increased due to the formation of a vacancy was calculated. The VFE for each configuration was calculated by using the equation (5):

$$E_{vac} = E_f - E_i + E_{coh} \quad (5)$$

here, E_{vac} = vacancy formation energy, E_f = energy of the system after the formation of vacancy, E_i = energy of the system before the formation of vacancy, E_{coh} = cohesive energy of the system

In the same way, the IFE can also be estimated, with the difference that in place of deleting, an extra atom was included to Nb bi-crystal. IFE for each configuration will be calculated by using the equation (6):

$$E_{int} = E_f - E_i - E_{coh} \quad (6)$$

CHAPTER 4

RESULTS AND DISCUSSION

As, discussed in the previous chapter, various molecular dynamics based simulations were carried out during the studies and the results obtained are discussed in the current chapter. The snapshots of the grain boundaries, their corresponding energies and their trend obtained is plotted in this chapter.

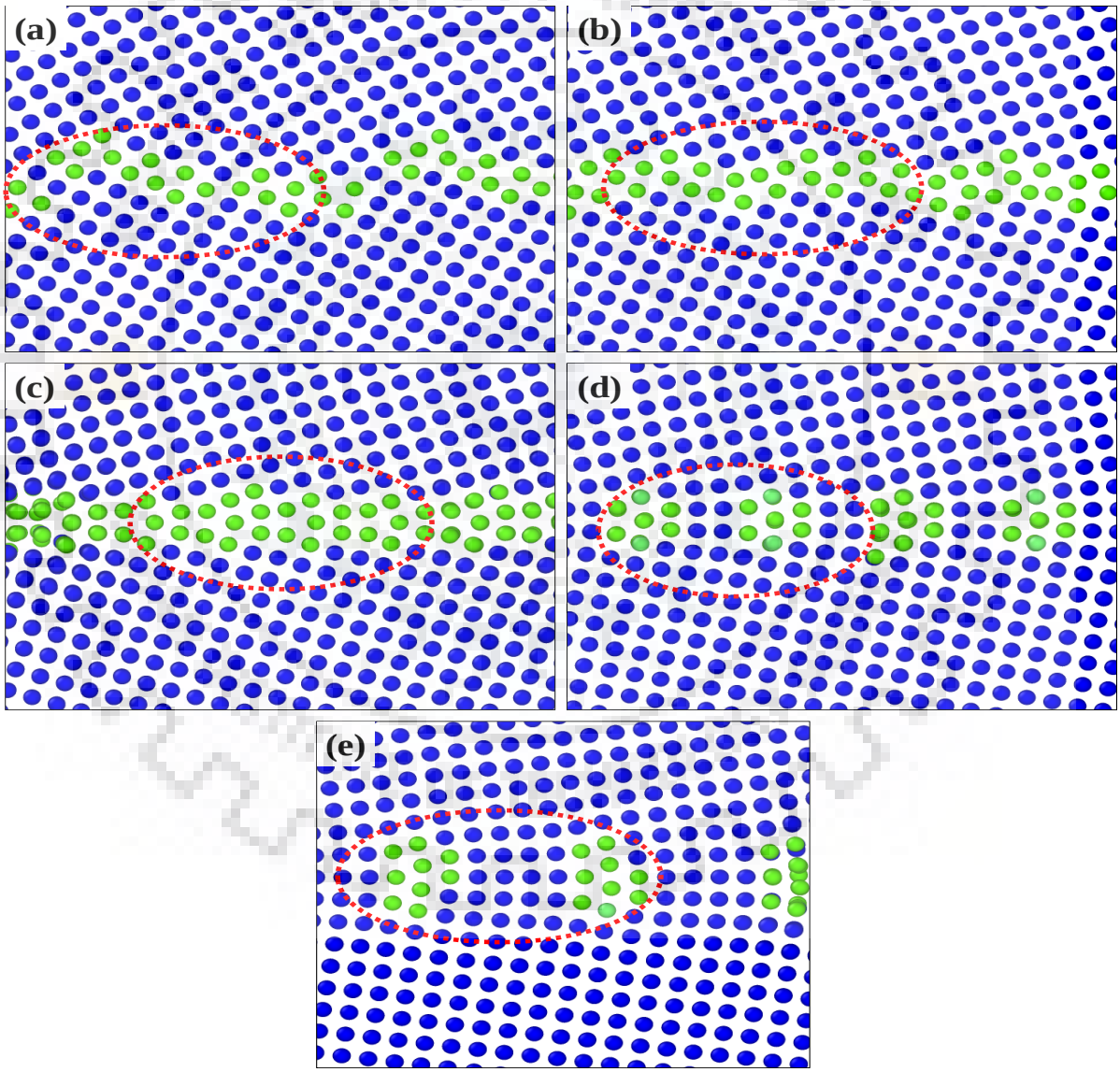

Figure 26: STGB structures with [0001] as the tilt axis containing mis-orientation angles (a) 25.06º (b) 43.6º (c) 53.13º (d) 67.38 (e) 73.73 (blue and green atoms correspond to perfect bcc crystal and GB atoms respectively- repetitive GB structures are encircled)

Figure 26, shows the snapshots of the STGB structures with [0001] as tilt axis for the various mis-orientation angles. The green atoms in the snapshots represent the grain boundary atoms which are not in the perfect bcc crystal form. The encircled atoms represent the repetitive grain boundary structures. The blue atoms here, corresponds to the perfect bcc crystal.

Table 4: Variation in GB energy with respect to mis-orientation angle

S.No.	Mis-orientation angle (2θ)	STGB energy (mJ/m^2)
1.	**0**	**0**
2.	**22.61**	**1281.689**
3.	**25.06**	**1299.782**
4.	**36.86**	**1334.094**
5.	**43.6**	**1270**
6.	**53.13**	**1305.517**
7.	**67.38**	**1246.205**
8.	**73.73**	**1123.662**
9.	**90**	**0**

From the above table we can see that the grain boundary energy at the mis-orientation angles of 0^o and 90^o is zero. This is attributed to the fact that at both these angles, there is no grain boundary formation or we can say that we get a structure like the single crystal. We can also infer that the there is a sharp increase in the grain boundary energy at 22.61^o and after that the GB energy variation is very little.

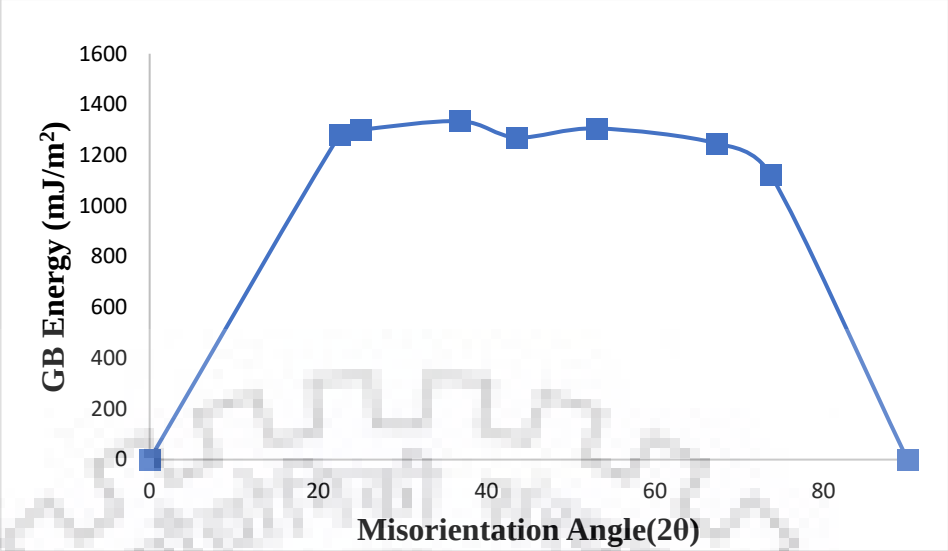

Figure 27: Variation in STGB energy with respect to mis-orientation angle along [0001] tilt axis.

Figure 26, shows the STGB structures with [0001] as tilt axis and their corresponding grain boundary energies are plotted in the figure 27. In figure 26, the first few snapshots represent the low angle tilt GBs with the misorientation angles in the range from 22.61° to 67.38°, whereas the other snapshots represent the high angle grain boundary structures. In figure 26(d), we can see the small formation of dislocation cores and it can be clearly seen in the figure 26(e), whereas in low angle grain boundaries, these dislocation cores are not visible because they merge into each other. From figure 27, it can be concluded that at lower tilt angles the increase in the grain boundary energy is more substantial and as there is increase in the tilt angle, it becomes almost saturated after 22.61°. Due to the four-fold symmetry of bcc crystal structure about [0001] as the tilt axis, the crystal structures at misorientation angles of 0° and 90° are in co-incidence and as a result, the GB energy reduces to zero. The GB energy at the misorientation angle of 36.86° is maximum and at 73.73° is minimum. This can be attributed to the fact that at 36.86° the GB structure is more incoherent than the GB structure at 73.73°.

In addition to the STGB, ATGB structures with misorientation angle of 36.86° along [0001] tilt axis are also shown in the figure 28. To generate the ATGB structures, two crystals on either side of them with a given mis-orientation angle were rotated with an inclination angle (Ø) in a clockwise direction. Due to this rotation the mis-orientation angle between the two crystals is also maintained. The variation of ASTGB energies for a constant mis-orientation angle of 36.86° and with the inclination angles (Ø) is shown in the figure 29.

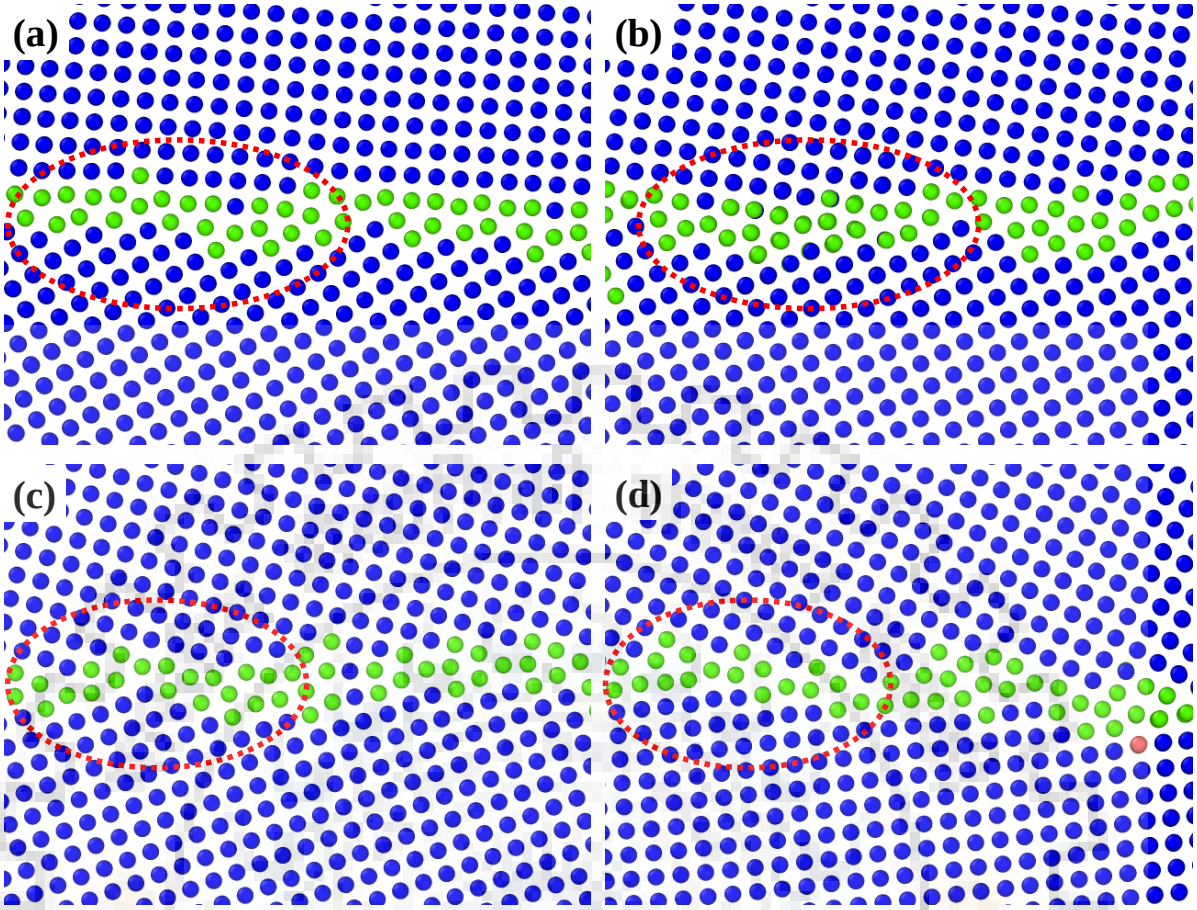

Figure 28: ATGB structures with misorientation angle (2θ) of 36.86º along the [0001] tilt axis and inclination angles (Ø) of (a) 30.96º (b) 36.86º (c) 43.6º (d) 53.13º

Figure 28, clearly depicts the snapshots of the ATGB structures with mis-orientation angle of 36.86º along the [0001] as the tilt axis with various inclination angles. From the figure, we can clearly say that the asymmetrical grain boundary structures are more disordered as compared to the symmetrical grain boundary structures. The green atoms in the snapshots represent the grain boundary atoms and the encircled atoms depict the repetitive grain boundary structures. The grain boundary atoms (green) does not follow the perfect bcc crystal structure while the other (blue) atoms does. The dis-orderliness in the GB structure is the result of the asymmetric orientation of the two crystals of the bcc Nb.

In table 5, the ATGB energies and their corresponding STGB energies are tabulated. We can see from the table 5, that the ATGB energy is maximum for the inclination angle of 30.96º. This is attributed to the most dis-ordered GB structure at this inclination angle, which is clearly visible in the figure 28 (a).

Table 5: ATGB energies with changing inclination angle and a constant mis-orientation angle of 36.86°

S.No.	Inclination angle (Ø)	ATGB energy (mJ/m^2)	Corresponding STGB energy (mJ/m^2)
1.	30.96	1415.663	1334.094
2.	33.69	1384.184	1334.094
3.	36.86	1366.21	1334.094
4.	43.60	1393.893	1334.094
5.	53.13	1413.452	1334.094

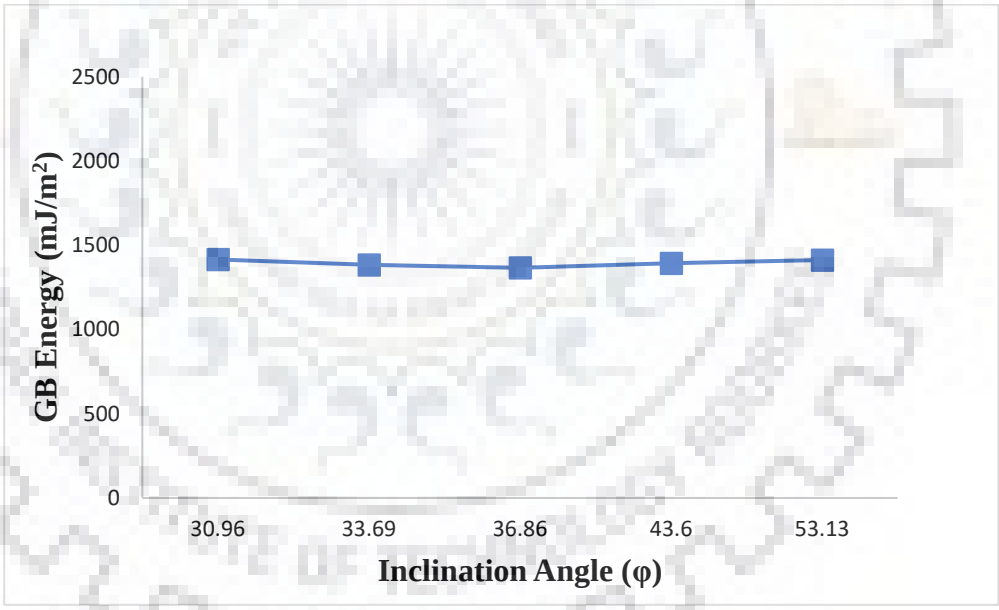

Figure 29: Asymmetrical tilt GB energies at mis-orientation angle of 36.86° as a function of inclination angle (Ø).

From figure 28, we can infer that the ATGB structures are comparatively more disordered than the STGB structures. This disordered structure can be attributed to the fact that the rotation of two crystals of the bi-crystal is in the same direction with the inclination angle (Ø). This incoherent structure of the GB is the reason for the higher GB energies in ATGB structures as compared to the STGB structures. Trend of ATGB energies is plotted in the figure 29.

4.1 Variation of VFE:

The variation of vacancy formation energy as a function of distance from grain boundary is plotted in the figure 30 and 31.

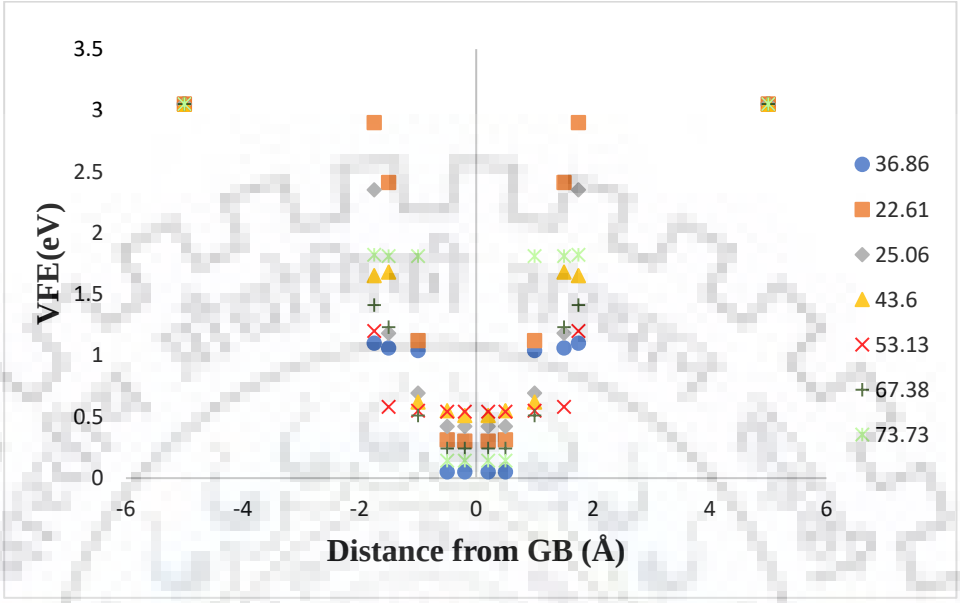

Figure 30: Variation of VFE as a function of mis-orientation angle, and distance from grain boundary for STGB with [0001] as the tilt axis.

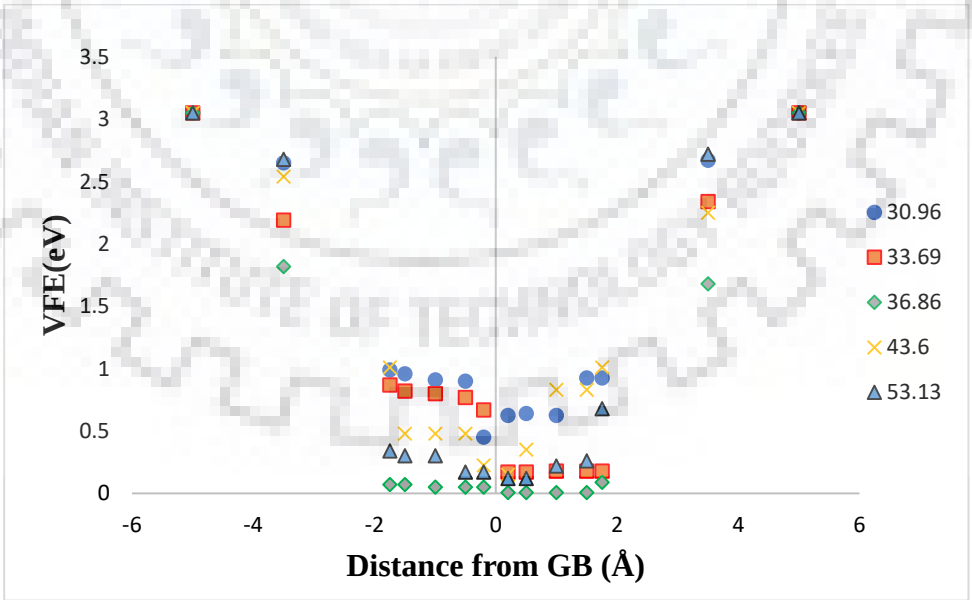

Figure 31: Variation of VFE as a function of the mis-orientation angle, and the distance from the grain boundary for ATGB with [0001] as the tilt axis.

From figures 30 and 31, it can be easily observed that the value of VFE decreases as we approach the GB, for both STGB as well as ATGB structures and it is independent of the mis-orientation angle. This can be attributed to the fact that at the grain boundary, the structure is incoherent as compared to the structure in the bulk. It can also be inferred that the value of VFE in the bulk, i.e. at a certain distance from the GB is approximately equal to 3.1 eV, which is same as found out for the single crystal. The VFE in close proximity to the GB approaches to zero, which is clearly visible from the plots. For the ATGB structures the VFE for most of the inclination angles is closer to the zero, as can be seen in the plot. This is so because for the ATGB structures the incoherency is more in GB structure, which means the GB energy is higher and as a result of that the VFE required is less as compared to the STGB structures.

4.2 Variation of IFE:

The plots below shows the variation of interstitial formation energy with distance from the grain boundary, both for the STGB and ATGB structures.

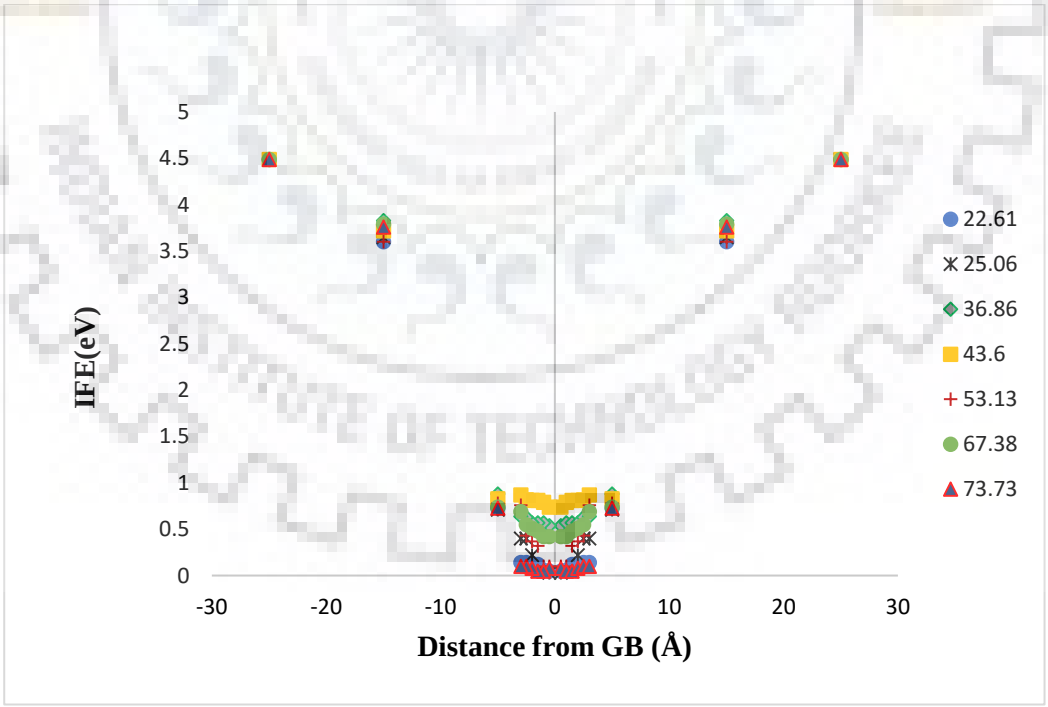

Figure 32: Variation of VFE as a function of mis-orientation angle, and distance from grain boundary for STGB with [0001] as the tilt axis.

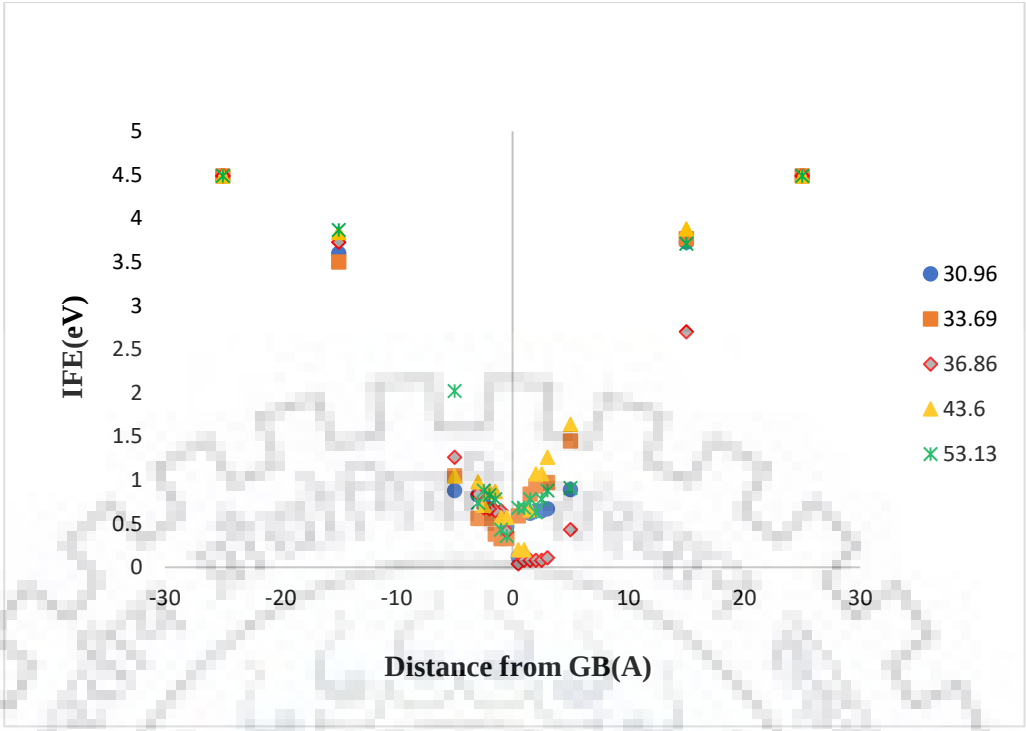

Figure 33: Variation of VFE as a function of mis-orientation angle, and distance from grain boundary for ASTGB with [0001] as the tilt axis.

From the figures 32 and 33, it can be inferred that the IFE keeps on decreasing as we move closer and closer to the grain boundary. This is similar to the case of VFE, that due to the presence of incoherency in the structure near the grain boundary, the IFE value decreases on approaching the grain boundary. The difference is in the bulk values of the VFE and IFE. The value of IFE in the bulk is more as compared to the VFE for the same GB structure.

4.3 Variation of VFE and GBE:

From the figure 34, it can be inferred that the minimum VFE for asymmetrical tilt grain boundaries decreases with increase in the grain boundary energy. This can be attributed to the fact that due to higher GB energy atoms are already in a higher energy state, thus the energy required to displace an atom from its lattice position decreases with increase in the GB energy.

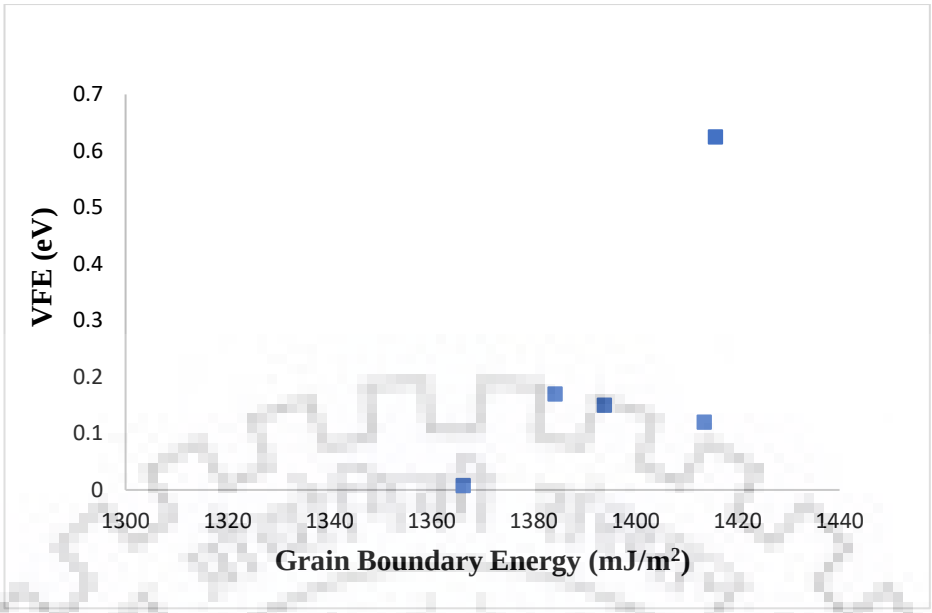

Figure 34: The trend of min. VFE as a function of GB energy for asymmetrical tilt GB with [0001] as the tilt axis.

4.4 Variation of VFE with mis-orientation angle:

Figure 35 and 36, represent the variation of VFE w.r.t. the mis-orientation angles for symmetrical and asymmetrical tilt GBs respectively. From figure 35, we can infer that there is no particular trend for the symmetrical tilt GBs while there is a decrease in the VFE with the mis-orientation angle for the asymmetrical tilt GBs.

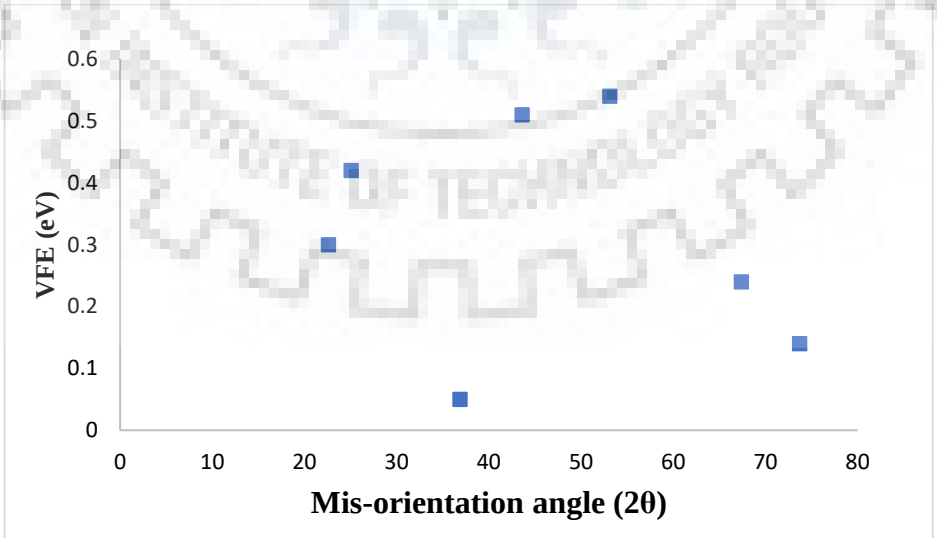

Figure 35: Trend of VFE as a function of mis-orientation angle for symmetrical tilt grain boundary tilted along the axis aligned with [0001].

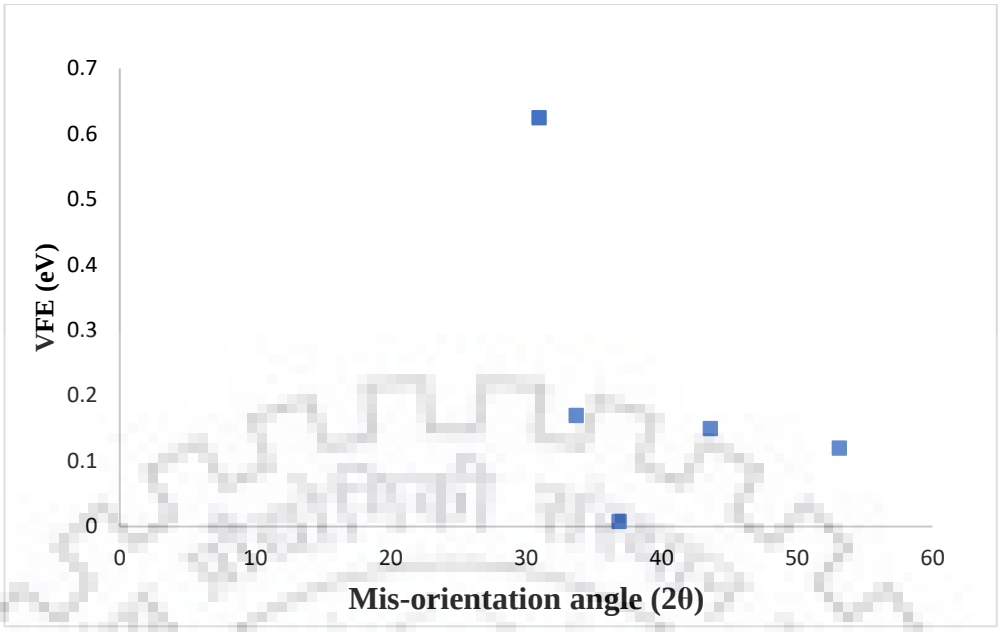

Figure 36: Trend of VFE as a function of mis-orientation angle for asymmetrical tilt grain boundary tilted along the axis aligned with [0001].

4.5 Vacancy Migration Energy:

Vacancy migration energy is the energy required to move a vacancy created in Nb crystal from one lattice position to another. This motion of vacancy is accomplished by using the nudged elastic band (NEB) algorithm. NEB is a method which is used to find both atomic configuration and energy barrier associated with the transition state. For example, when a atom moves from its lattice position to the another lattice position in a co-ordinated fashion with the neighbouring atoms, it requires to perform a diffusive hop to get through various energy basins. This movement of atom describes a transition path. In NEB algorithm, the calculations are performed by considering the multiple replicas of the system. The first and the last replicas are end points of transition path. In order to calculate VME, a vacancy was created either in bulk or near the GB. The position of the vacancy is defined as atomic coordinate for final replica. In order to replicate migration of the vacancy, the nearest neighboring atom to the vacancy was moved towards the vacancy, in step-wise fashion with the help of multiple replicas used in between first and end replicas. The trend obtained for the VME is plotted in the graphs below.

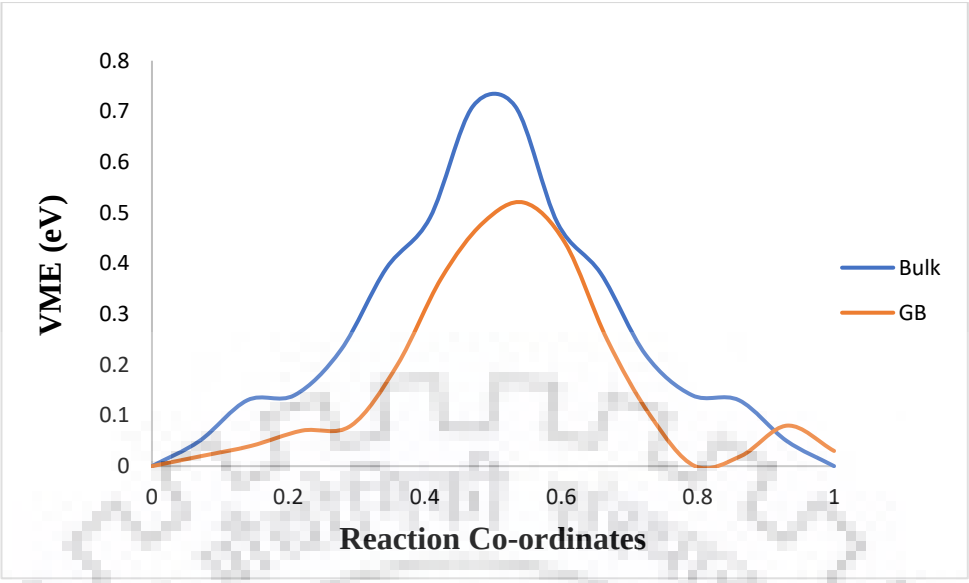

Figure 37: Minimum vacancy migration path in a bi-crystal of Nb containing a STGB with mis-orientation angle of 36.86 and inclination angle 36.86°.

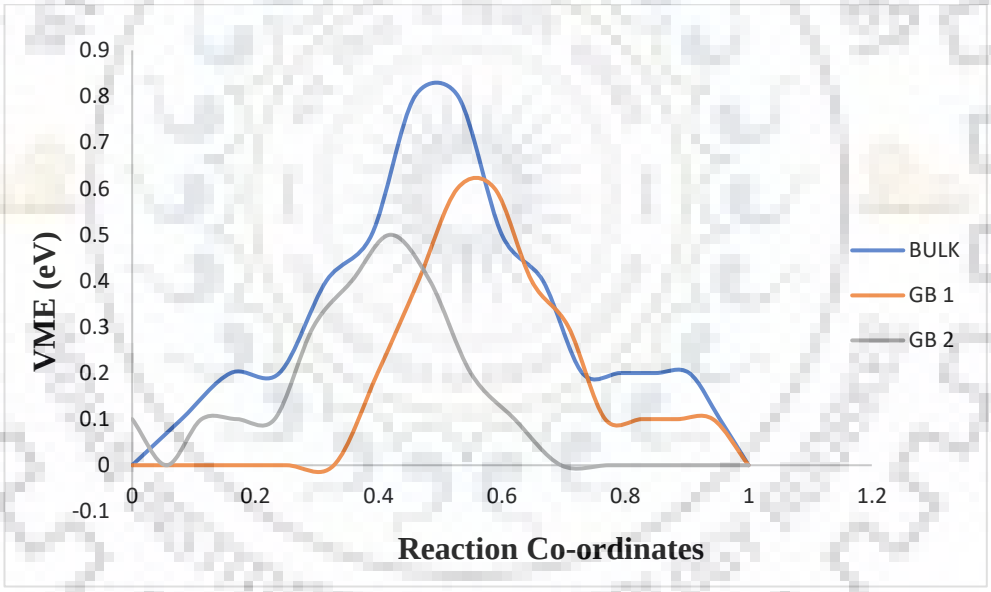

Figure 38: Minimum vacancy migration path in a bi-crystal of Nb containing a ATGB with mis-orientation angle of 36.86 and inclination angle 36.86°.

From the figures 37 and 38, it can be observed from the plots that the VME in close proximity of the GB is lower as compared to bulk values. VME was estimated in STGB and ATGB configuration, containing mis-orientation angle of 36.86° and minimum energy path is plotted in Fig.38. The value of VME = 0.71eV estimated in bulk is validated with the literature, and is same in STGB and ATGB configurations. We can infer from the plot in Fig.38 that VME

values drastically decreases in the vicinity of GB plane, and this is independent to configuration of GB. This is due to the fact that the atomic structure near the grain boundary is incoherent as compared to bulk. The trend obtained with VME is similar to the trend obtained with VFE and IFE.

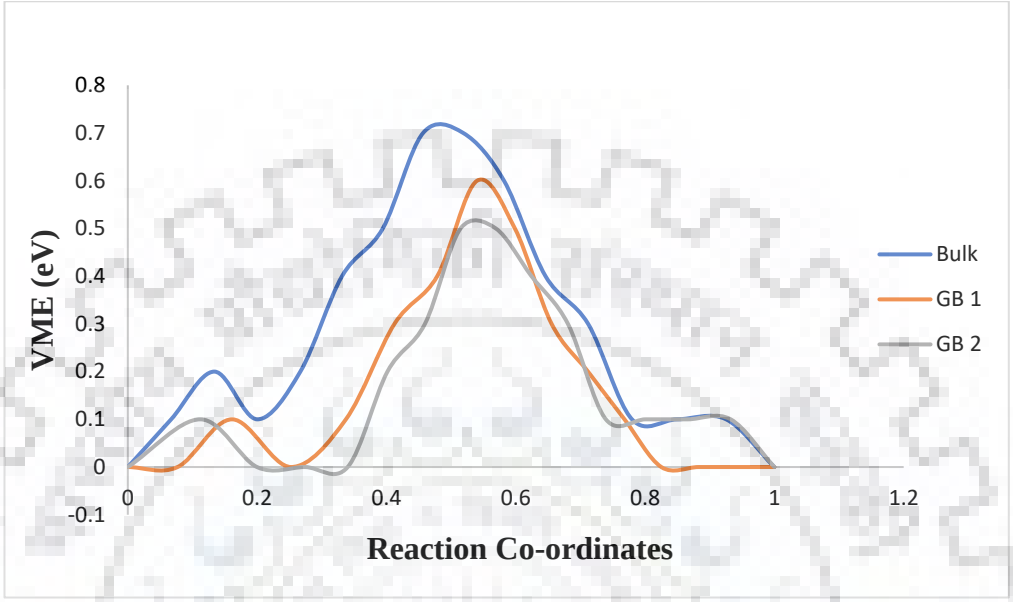

Figure 39: Minimum vacancy migration path in a bi-crystal of Nb containing a ATGB with mis-orientation angle of 36.86 and inclination angle 36.86°.

Figure 39, is also representing the plot for the VME for the reaction co-ordinates taken on the other side of the grain boundary. The trend is almost similar to that obtained in the figure 38, with the difference that the VME for the vacancy near the GB has a much sharper decrease in the figure 38. Also, in both the figures 38 & 39, the trend of VME for the vacancy created in the bulk is almost similar.

CHAPTER 5

CONCLUSION AND FUTURE ASPECTS

In this dissertation work, grain boundary structures were created along [0001] as the tilt axis for the bi-crystal of Nb. Both the STGB and ATGB were created, and their effect on generated radiation-induced point defects was studied. It is established from this thesis work that grain boundary structures have a substantial impact on formation and distribution of the radiation-induced point defects. The defect formation energy i.e. VFE is same in the bulk as the single crystal but decreases on moving close to the grain boundary and it is in accordance with the experimental results obtained previously by the researchers. Various simulations were done to study the interstitial formation energies (IFE) in conjunction with the grain boundary configuration. The interstitial formation energy was also estimated through the simulations and validated with the experimental results. Nudged elastic band algorithm was used to estimate the vacancy migration energies (VME) in conjunction with different types of grain boundaries configurations. This involved movement of vacancies in the form of several replicas, which together make a transition path.

Molecular dynamics-based simulation eliminates the time and spatial scale and cost concerns of experimental methods. Hence, Molecular dynamics-based approach is a viable alternative for experiments to study the effects of radiation.

These MD based simulations can be further extended towards the following future aspects:

- These can be utilized to study the effects of irradiation damage in the alloys of the metals like Zr-Nb alloy etc.
- MD based simulations can be used to study the phenomenon of fracture in the metals and their alloys and estimate their fracture toughness values.
- The molecular dynamics-based simulations can also be utilized in the multiscale modelling techniques to derive certain traction-displacement laws while studying the fracture of the material.

REFERENCES

1. S.J. Wooding, D.J. Bacon, 1997, a molecular dynamics study of displacement cascade in α- Zirconium, Philosophical Magazine A, Vol. 76, No. 5, 1033-1051.
2. https://www.nature.com/articles/srep21034 (8/4/2018;10:42a.m.)
3. Kwon, J., Kim, W., Hong, J.H., 2006. Comparison of the primary damage states in iron and nickel by molecular dynamics simulations. Radiat.Eff. Defects Solids. 161, 207-218.
4. Stoller,R.E., Odette,G.R., Wirth,B.D., 1997. Primary damage formation in bcc iron. J.Nucl.Mater. 251, 49-60.
5. Victoria, M., Baluc, N., Bailat,C., Dai,Y., Luppo, M.I., Schaublin, R., Singh, B.N., 2000. The microstructural and associated tensile properties of irradiated fcc and bcc metals. J.Nucl.Mater. 276, 114-122.
6. Wooding, S.J., Howe, L.M., Gao, F., Calder, A.F., Bacon, D.J., 1998. A molecular dynamics study of high energy displacement cascades in α-zirconium.J. Nucl. Mater. 254, 191-204.
7. Wooding, S.J., Bacon, D.J., 1995. A computer simulation study of displacement cascades in α-zirconium. Philos.Mag.A.72, 1261-1279.
8. June Gunn Lee, Computational Materials Science, An Introduction, CRC Press, Taylor & Francis Group, 2015
9. M.R. Fellinger, H. Park, J.W. Wilkins, Force-matched embedded atom method potential for niobium, Phys. Rev. B.Condens. Matter 81 (2010) 144119.
10. Avinash Parashar, Divya Singh, 2017, Molecular dynamics based study of an irradiated single crystal of niobium. Computational materials science,131, 48-54.
11. https://en.wikipedia.org/wiki/Molecular_dynamics#Design_constraints (21/4/2019; 3:07 p.m.)
12. http://www.chemistrylearner.com/zirconium.html (8/4/2018;10:41a.m.)
13. https://www.greatmining.com/niobium.html (8/4/2018;10:41a.m.)
14. https://www.alibaba.com/product-detail/R060705-zirconium-niobium-alloy-tube-china_60714166434.html (8/4/2018;10:42a.m.)
15. https://en.wikipedia.org/wiki/Niobium (21/4/2019; 3:24 p.m.)

16. R.P. Tucker, M.S. Wechsler, S.M. Ohr, Dislocation channeling in neutron irradiated niobium, J. Appl. Phys. 40 (1969) 400–408.
17. Divya Singh, Avinash Parashar, 2017, Effect of symmetrical and asymmetrical tilt grain boundaries on the tensile behaviour of bcc-Niobium. Computational materials science,143, 126-132.
18. A.C. Lewis, C. Eberl, K.J. Hemker, T.P. Weihs, GB strengthening in Copper/Niobium multi-layered foils and fine grained Niobium, J. Mater. Res 23 (02) (2008) 376–382.
19. Z.C. Szkopiak, The Hall-Petch parameters of Niobium determined by the grain size and extrapolation methods, Mater. Sci. Eng. 9 (1972) 7–13.
20. B. Jóni, E. Schafler, M. Zehetbauer, G. Tichy, T. Ungár, Correlation between the microstructure studied by X-ray line profile analysis and strength of the high pressure-torsion processed Nb and Ta, Acta Mater. 61 (2013) 632–642.
21. Divya Singh and Avinash Parashar, 2018, Effect of symmetrical and asymmetrical tilt grain boundaries on radiation-induced defects in zirconium.
22. Rajesh Kumar, Avinash Parashar, (2016), Atomistic modelling of mechanical and thermal properties of BN nanofillers: a review. Nanoscale, 8,22-49.
23. Rajasekaran G., Avinash Parashar, (2016) Molecular dynamics based simulations to study the effect of modified cut-off function for Tersoff potential on estimating mechanical properties of graphene. Material research express , 3 , 035011.
24. Rajasekaran G., Avinash Parashar, (2016) Molecular Dynamics Study on Mechanical Response and Failure Behaviour of Graphene: Performance Enhancement via 5-7-7-5 Defects. RSC Advances,6, 26361-26373
25. Divya Singh, Avinash Parashar, Rajeev Kapoor, Apu Sarkar, A. Kedharnath (2019), Effect of symmetrical and asymmetrical tilt grain boundaries on the tensile deformation of zirconium bi-crystals: a MD based study. Journal of Materials science, 54, 3082-3095
26. https://www.indiamart.com/proddetail/niobium-alloy-11699066755.html (24/04/2019; 4.07 p.m.)
27. https://www.researchgate.net/publication/281811031_The_effect_of_dissolved_hydrogen_on_spent_nuclerar_fuel_corrosion/figures?lo=1 (24/04/2019; 4.07 p.m.)
28. https://phys.org/news/2017-01-discovery-jet-hotterand-cleaner.html (24/04/2019; 4.10 p.m.)

29. https://www.swagelok.com/en/product/Tubing-and-Tube-Accessories (24/04/2019; 4.10 p.m.)
30. http://www.scienceindia.in/home/view_blog/33 (24/04/2019; 4.15 p.m.)
31. Butcher et al, Cindy L. Routree and Priya Vashistha, "Atomistic plasticity: description and analysis of a one billion atom simulation of ductile materials failure", Computational Methods Appl. Mech. Engg. 193 (2004) 5257-5282, 2002.
32. S. Namilae, N. Chandra, T.G. Nieh, "Atomistic simulation of grain boundary sliding in pure and magnesium doped aluminium bi-crystals" Scripta Materialia 46 (2002) 49-54.
33. C. Zheng and Y.W. Zhang, "Atomistic simulations of mechanical deformation of high-angle and low-angle nanocrystal line copper at room temperature" Materials Science and Engineering A 423 (2006) 97-101.